An Observer Based Approach to Force Reflecting Bilateral Teleoperation

by

Duruhan Özçelik

Submitted to the Graduate School of Sabancı University
in partial fulfillment of the requirements for the degree of
Master of Science

Sabancı University

August, 2011

An Observer Based Approach to Force Reflecting Bilateral Teleoperation

APPROVED BY:

Assoc. Prof. Dr. Mustafa Ünel (Thesis Advisor)	.....
Prof. Dr. Asif Sabanovic	.....
Assoc. Prof. Dr. Kemalettin Erbatur	.....
Assist. Prof. Dr. Volkan Patoğlu	.....
Assist. Prof. Dr. Hakan Erdoğan	.....

DATE OF APPROVAL: 03/08/2011

An Observer Based Approach to Force Reflecting Bilateral Teleoperation

Duruhan Özçelik

ME, Master's Thesis, 2011

Thesis Supervisor: Assoc. Prof. Mustafa Ünel

Keywords: Bilateral teleoperation, communication delay, predictor observer, disturbance observer, reaction torque observer, four channel architecture

Abstract

Bilateral teleoperation systems are an active area of research with possible applications in healthcare, remote surveillance and military, space and underwater operations, allowing human operators to manipulate remote systems and feel environment forces to achieve telepresence. The physical distance between the local and remote systems introduces delay to the exchanged signals between the two and cause instability in the bilateral teleoperation. With the advent of the internet, possible applications of bilateral teleoperation systems have proliferated, growing the interest and amount of research in the field.

The delay compensation method for stable and force reflecting teleoperation proposed in this thesis is based on utilization of three different types of observers: A novel predictor observer that estimates the undelayed states of the remote system based on a nominal model, disturbance observers that eliminate internal and external disturbances and linearize the nonlinear dynamics of the two systems, and reaction torque observers that estimate the net external forces on the two systems. The controller for the remote system is placed at the local site, along with the predictor observer and the control input is sent to the remote system through the communication channel. Force reflection is achieved using a modified version of the 4-channel architecture where control input and position of the remote system and the environment force estimations are exchanged between the two systems. Performance of the proposed method is tested with Matlab/Simulink simulations and compared to two other methods in the literature. Real-time experiments under variable communication delay are also performed where the delay is

both artificially created using Matlab/Simulink blocks and obtained via the internet by bouncing signals off a remote computer outside the Sabancı University campus. Both the simulations and experiments are executed on a pair of 1-DOF robot arms and a pair of 2-DOF pantograph robots. The results show that stable and force reflecting teleoperation is achieved with successful tracking performances of the remote system.

Kuvvet Yansımalı İki Yönlü Teleoperasyona Gözlemci Tabanlı Bir Yaklaşım

Duruhan Özçelik

ME, Master Tezi, 2011

Tez Danışmanı: Doç. Dr. Mustafa Ünel

Anahtar Kelimeler: İki yönlü teleoperasyon, iletişim gecikmesi, kestirici gözlemci, bozucu gözlemcisi, tepki torku gözlemcisi, dört kanallı mimari

Özet

İki yönlü teleoperasyon sistemleri, sağlık, uzaktan gözetim, askeri, uzay ve sualtı faaliyetleri alanlarında uygulamaları olan aktif bir araştırma alanıdır. Bu sistemler, insan operatörlerin uzaktaki sistemleri kontrol etmelerini ve bu sistemlere uygulanan çevresel kuvvetleri hissederek uzakta bulunmalarını sağlar. Yakın ve uzak sistemler arasındaki fiziksel mesafe paylaşılan sinyallerde gecikmeye ve sistemde kararsızlığa neden olur. İnternetin yayılması sonucu iki yönlü teleoperasyon sistemlerinin muhtemel uygulama alanlarının artması konu üzerine ilgi ve araştırmaların artmasına sebep olmuştur.

Bu tezde kararlı ve kuvvet yansımalı teleoperasyon için önerilen zaman gecikme telafi yönteminde üç adet gözlemci kullanılmıştır: Uzaktaki sistemin, nominal bir model kullanarak, gecikmemiş durumlarını tahmin eden bir kestirici gözlemci, sistemlere etki eden dahili ve harici bozucu etkileri kestirip ortadan kaldıran ve böylece sistemleri doğrusallaştıran bozucu gözlemcileri ve sistemlere etki eden net harici kuvveti tahmin eden tepki torku gözlemcileri. Uzak sistemin denetleyicisi, kestirici gözlemci ile birlikte yakın tarafa konmuş ve uzak sistemin denetim girdisi iletişim kanalından gönderilmiştir. Kuvvet yansıması, 4-kanallı mimarinin modifiye edilmiş bir haliyle, uzak sistemin denetim girdisi, pozisyonu ve kestirilen çevre kuvveti paylaşılarak sağlanmıştır. Önerilen yöntemin performansı Matlab/Simulink simülasyonlarında test edilmiş ve literatürdeki iki farklı yöntemle karşılaştırılmıştır. Yöntem, zaman gecikmesinin Matlab/Simulink ortamında yaratıldığı ve sinyallerin internet üzerinden Sabancı Üniversitesi kampüsü dışındaki bir bilgisayardan yansıtılarak gerçek gecikmelerin kullanıldığı gerçek zamanlı deneylerle de test

edilmiştir. Hem simülasyonlarda hem de deneylerde bir serbestlik dereceli robot kolu ve iki serbestlik dereceli pantograf robot çiftleri kullanılmıştır. Sonuçlarda kararlı ve kuvvet yansımalı teleoperasyon sağlandığı ve uzak sistemin takip performansının başarılı olduğu gözlemlenmiştir.

Acknowledgements

It is a great pleasure to extend my gratitude to my thesis advisor Assoc. Prof. Dr. Mustafa Ünel for his precious guidance and support throughout my Master's study.

I would like to thank Prof. Dr. Asif Sabanovic, Assoc. Prof. Kemalettin Erbatur, Asst. Prof. Volkan Patoğlu and Asst. Prof Hakan Erdoğan for their feedbacks and spending their valuable time to serve as my jurors.

I would like to acknowledge the financial support provided by TUBITAK (The Scientific and Technological Research Council of Turkey) through the project "Bilateral control systems with time delay compensation" under the grant 106M533.

I would sincerely like to thank to bilateral teleoperation project members Tuğba Leblebici and Serhat Dikyar for their pleasant team-work and providing me the necessary motivation during hard times. I would also like to thank all mechatronics laboratory members I wish I had the space to acknowledge in person, for their great friendship throughout my Master's study.

Last but not least, I would like to thank my family for all their love and support throughout my life.

Contents

List of Figures

List of Tables

Chapter I

1 Introduction

Robots have replaced humans in many repetitive and practical tasks such as welding, painting, vacuuming, lawn moving, etc. However more sophisticated tasks require a blend of robotic manipulation and human perception. Robotic surgery, bomb diffusion and remote surveillance are examples of such tasks where human operators manipulate robots in environments that are hazardous, difficult, too distant or require too much precision to work in. A system that enables real-time control of remotely located machines by a human operator is called a teleoperation system. A teleoperation system consisting of two identical or functionally similar machines at both ends it can be called a bilateral teleoperation system. If the operator is able to feel the forces present at the remote site, then the operation is called telepresence.

Bilateral teleoperation systems can be modeled as consisting of five elements: Operator, master (local) system, communication channel, slave (remote) system and environment. Different signals can be shared amongst the two systems to accomplish the two goals of bilateral systems: stability and transparency. Stability refers to stable tracking of the master position by slave system and transparency refers to successful reflection of environment forces to the operator. In the literature, different methods are proposed to share master and slave position, velocity and force information.

The physical distance between the master and slave systems causes delays in the exchanged signals which is the reason of the main problem in bilateral systems: instability. Time delay implies infinite dimensional systems and injects energy to the exchanged signals that causes the instability. Whether there is a reliable communication channel between the two systems where the amount of delay is known or the signals are shared over an unreliable connection like the internet with unpredictable delays, bilateral systems require a delay compensation technique in order to deliver stable and transparent operation.

1.1 Motivation

Bilateral teleoperation systems enable humans to manipulate remote environments that are otherwise difficult or dangerous to access or inaccessible in a safe and effortless manner. For example sending a remote controlled robot to a deep sea research task at a depth of 5000 m, where the atmospheric pressure reaches 500 atm, instead of building a vessel that will withstand the pressure and ensure the safety of the people is definitely a less expensive and safer option. This example can be extended to a repair task that take place in space, a bomb diffusion task or a waste disposal task that takes place in a radioactive zone. In other tasks, such as robotic surgery (Fig. 1.1), bilateral systems are used to enhance the precision of the human operator. Robotic telesurgery on the other hand, enables a surgeon to operate on a patient in a different city or country without either of them spending time to adjoin in an operating room.

There are examples of teleoperation systems that achieve some of these tasks within a limited distance, but as the amount of communication delay

Figure 1.1: da Vinci surgical system

increases with increasing physical distance between the operator and remote system, stable and transparent teleoperation across great distances becomes a challenge. Numerous researchers have published their work on stable and transparent teleoperation since the first introduction of the problem in 1950s and it continues to be an area of active research. With further advancements in the area and the continuing growth of connectivity around the globe via the internet, it is not a farfetched assumption that bilateral teleoperation systems will enable humans to experience telepresence in the future. Aside from dramatic advancements such as telesurgery systems, human controlled humanoid robots, even a mundane one such an online shopping website that allows its users to interact with their products much like a physical store through the use of a bilateral system is an exciting view of the future.

The complexity of some of these tasks render the current research elementary, consisting of limited degree-of-freedom stationary systems. Advancements in the area are necessary for complex techniques that control

several multi degree of freedom manipulators simultaneously and send accurate visual and force feedback to the operator for a realistic telepresence operation.

1.2 Literature Review

The earliest work on the stability of bilateral systems under delay is by Sheridan and Ferrell [1]. The authors experimented with a pair of "servo-controlled minimal manipulators" and concluded that stable operation can be achieved by adopting a simple strategy of moving open loop and then waiting for correct feedback [1]. Although a pioneering work in the field, transparency is not addressed by the authors. Ferrell considered force feedback and transparency in his subsequent works [2], [3] and experimentally concluded that delays in the magnitude of 100 ms cause instability in the bilateral system.

Theoretical works on stability of systems under time delay started being produced after a relatively long period of time. In 1988 Anderson and Spong published their groundbreaking work [4], which utilizes the so-called "scattering operator" to prove that the communication channel is not passive and injects energy to the system and introduces the "scattering transformation", which renders the system passive, thus stable, by dampening the energy injected by time delay. In their subsequent work, the authors proved the asymptotic stability of scattering transformation [5]. Their work inspired other researchers to produce passivity based methods. In 1991, Niemeyer and Slotine extended the scattering theory by introducing "wave variables" [6]. In this technique, velocity and force signals are converted to wave variables using wave transformation before they are sent through the communication

channel. Authors propose different techniques for achieving passivity using wave variables: imitating natural wave phenomena, matching the wave impedance, wave filtering and using wave variable predictors. The stability of these techniques are proven in the framework of passivity theory. The authors analyze the transient behavior of the bilateral system and develop a tuning mechanism to adjust the tradeoff between telepresence and operation speed [7].

With the advent of the internet in the 1990s, possible applications of bilateral systems increased drastically. The internet provides an inexpensive data route between great distances and the infrastructure has been constantly growing and improving since its inauguration in the early 1990s. With its packet switched network it eliminates the need for building a dedicated communication channel between bilateral systems. However, in a packet switched network data may be transferred through inconsistent routes or the traffic volume at a given instant through the channel may slow down transmission speeds and affect the amount of delay between master and slave systems. Since the previous research in the area considered a dedicated communication channel and constant delay, the variable delay characteristic of the internet necessitated new methods to overcome the stability problem.

One of the earliest works on compensation of variable delay was by Kosuge et al. [8]. In their work the authors propose a straightforward method to measure the maximum delay in the communication channel T_c and buffer delayed signals until the delay is equal to T_c. They achieve this by sending a timestamp along with exchanged signals. With this method they ensure a constant delay and use scattering transformation to make the system passive. In 1997, Oboe and Fiorini investigated the detrimental effects of variable de-

lay on teleoperation [9]. In their work they compare Transmission Control Protocol (TCP) and User Datagram Protocol (UDP) and provide a model for internet connection so that existing control methods can be simulated under variable delay. They developed a design environment for the identification, control design and test of teleoperation systems connected to the internet [10] in 1998. Niemeyer and Slotine extended their wave variables technique to account for variable delays by applying reconstruction filters to the delayed signals [11]. The filters utilize the integrals of both the wave variable u and its square u^2 to reconstruct distorted wave variable signals and achieve stable and transparent teleoperation. In 2002, Lozano et al. proposed a modified scattering transformation method to provide passivity under variable delay [12]. The proposed method introduces two time-varying damping coefficients to the scattering operation in order to dissipate the energy injected by delay and achieve stable tracking of the master by slave with force reflection. In 2003, Chopra et al. proposed a similar method to achieve stable and transparent teleoperation under variable delay by adding time-varying damping coefficients to the scattering operation [13]. Chopra et al. extended their work in 2004 by proposing an "adaptive coordination control" scheme based on a passivity framework [14]. The method uses state feedback to define a new passive output for the master and slave robots containing both position and velocity information to "kinematically lock" the master and slave. The results presented in their work show that stable and transparent teleoperation is achieved under variable delay.

Another shortcoming of packet switched networks is packet loss. Packet loss can be caused by signal degradation, channel congestion, corrupted packets, faulty network hardware or other factors. Numerous studies have been

produced to investigate the effects of lost packets on the teleoperation and compensate for them. Secchi et al. proposed a passive linear interpolation scheme where lost packets are interpolated from received ones [15]. The method requires a buffer of signals greater than maximum number of consecutive lost packets, thus a priori knowledge about the communication channel. By keeping a buffer, the receiver stores the future values of incoming signals and can interpolate missing values using these future values. Although this method provided a solution to the packet loss problem, the use of a buffer caused extra delay in the system. Beretesky et al. proposed a solution to this problem in which missing data is interpolated from previous values in the buffer, thus eliminating the extra delay in the process [16]. In 2006, Mastellone et al. proposed a different approach to compensate for lost packets in the network [17]. By forming models of the master and slave systems, they estimated the missing states of the systems and fed the estimated states to their hybrid controller.

Other than the scattering and wave variable techniques presented previously, there are different approaches in the literature to provide passivity under delay conditions. Park and Cho proposed a sliding mode based controller with a nonlinear gain independent of the variable delay and showed that the proposed method compensates the delay in 1999 [18]. However, their method requires the maximum round-trip delay and the order of the environment force to be measured in advance and the gains set accordingly. In 2001, Cho et al. improved the sliding mode based controller to include an impedance model and eliminate the need for a priori knowledge on the delay charateristics [19]. In 2005, Chopra and Spong showed that exponential convergence of the master and slave positions can be achieved without

encoding the exchanged signals as scattering or wave variables [20]. The input forces were computed directly using the measured and received position and velocity data and sent through the communication channel. Over a series of publications, Lee and Spong devised a PD based control method for bilateral systems with multi DOF robots under constant delay [21] - [22]. The proposed control scheme passifies the communication and control blocks together - as opposed to previous works that passified them seperately - and guarantees energetic passivity of the closed-loop teleoperator. Although their method provided stable and transparent teleoperation, the constant delay assumption was unrealistic for its time, and it was improved in 2006 by the authors to compensate for variable delay as well. In order to achieve passivity in the two channels in unity the authors used controller passivity concept, the Lyapunov-Krasovskii technique and Parseval's identity. Nuno et al. refuted Lee and Spong's approach by claiming that a $\mathcal{L}_\infty$ stable mapping from velocity to force cannot be defined [23]. They showed that the passivity of PD like control structures can be achieved by injecting sufficiently large damping to the manipulator subsystems. In their simulations, they achieved stable and transparent control of the master and slave systems using delayed force or position signals. They concluded that large damping injections affected the tracking performance adversely. In their subsequent work, the authors developed a simple P-like and PD-like position controllers and proved their stability using Lyapunov analysis [24].

Transparency in a bilateral system is a crucial requirement for telepresence. Passivity based techniques concentrate on achieving stability by passifying the teleoperation systems, but many of them fail to deliver transparency in the system. In the early 1990s, it was independently shown by

Lawrence [25] and Yokokohji and Yoshikawa [26] that for achieving transparency in a bilateral system both the position and force information of the two systems need to be shared. This requires four information channels for master position and force and slave position and force, and the implementation was named 4-channel architecture. Both works concluded that in order to achieve perfect transparency in the bilateral system, the impedance felt by the operator should equal to the impedance of the environment. While Lawrence utilized the two-port "hybrid parameter matrix" to reach this conclusion, Yokokohji and Yoshikawa used the "chained matrix". Lawrence also concluded that stability and transparency are conflicting objectives in teleoperator system design and a tradeoff between the two exists. In 1995, Zhu and Salcudean developed on Lawrence's work to show that transparency can be achieved using the 4-channel architecture for systems that are driven by velocity control [27]. Zaad and Salcudean proposed a method for eliminating the need for force sensors and estimating the environment impedance from a model of the environment [28]. In their subsequent work the authors further improved their method by adopting an adaptive control method that does not require a priori knowledge of the master, slave, environment and operator impedances [29].

Prediction systems are proposed in various works for different purposes in bilateral teleoperation. Communication network models are utilized for determining delay characteristics of the communication channel, missing or delayed states of the master and slave systems are estimated using appropriate linear and nonlinear models, force predictors are used to eliminate the need for costly force sensors and disturbance observers are utilized in several works for linearizing system dynamics and rejecting internal and external

disturbances on the system. The Smith predictor, developed by Otto J. M. Smith in 1957 was first used for compensating "dead time" in 1959 [30]. In 2002, Arioui et al. proposed a modified Smith predictor for eliminating the time delay from the characteristic equation of the closed loop system and thus compensate for it [31]. Munir and Book integrated the modified Smith predictor with a Kalman filter and an energy regulator to provide passivity under constant and variable delay conditions [32],[33]. Shahdi and Sirouspour proposed a method that uses multi-model decentralized controllers for the master and slave systems that are fed with estimated states from the dynamical models of the systems [34]. The controllers implement a "Linear Quadratic Gaussian (LQG)" algorithm and switch between two controllers for free motion/soft contact and rigid contact. The authors developed their work by incorporating a parameter adaptation law to improve the estimation performance of the dynamical models and proved the stability of the proposed method using Lyapunov analysis [35], [36]. In 2009, Gadamsetty et al. proposed a sliding mode based novel observer to estimate the states of the remote system using a nominal model of the system and an extended Kalman filter based disturbance observer to linearize the remote system dynamics [37]. The control input driving the remote system is computed at the local site using the estimated states and a "PD+" controller and sent through the communication channel. This architecture creates an inevitable delay in the execution of the task at the remote site since the control input is computed locally but provides stable teleoperation.

Force observers are very practical in teleoperation systems. Acquisition of physical force sensors can be costly for many practical tasks, especially if the task does not require sensitive haptic feedback for completion. For

example loading a mobile surveillance robot sent to investigate the ruins of a building damaged by an earthquake with expensive force sensing equipment is unfeasible due to the high risk of losing the robot. Force sensors provide a software solution to force measurement. In 2005, Mobasser and Zaad developed a "Model-Independent Force Observer (MIFO)" that utilizes a multilayer perceptron neural network for force estimations at the master and slave systems [38]. The neural network is trained off-line with measured contact force and motor torque samples from the entire workspace of the robots and is used in real time to estimate force information during operation. Smith et al. proposed a new neural network based method, "Inverse-Dynamics NN (IDNN)" that uses the MIFO for motor torque estimations and uses the inverse dynamics of the robot to estimate force information [39]. The authors show that operator and environment forces can be estimated with 98.3% accuracy. Polushin et al. utilize "high-gain observer" to estimate the force information and use these estimations to drive the master and slave systems using novel "Force Reflection (FR)" [40], and "projection-based FR" algorithms [41]. In 2009, Daly and Wang proposed the use of "Unknown Input Observers" for estimating the force information of master and slave systems. The authors developed on earlier work by Cho et al. [19] and implemented the observers using the sliding mode theory liberating Park and Cho's early technique from the need for any a priori knowledge about the system or communication channel [42].

In their series of works, Natori, Ohnishi et al. developed a purely observer based technique for stable and transparent teleoperation. The authors first proposed the novel observer "Communication Disturbance Observer (CDOB)" in 2004 [43]. They claimed that CDOB treats time delay

in the communication channel as external disturbance and compensates it at the local site to feed the controller with undelayed position information of the remote system, and presented simulations where CDOB is implemented and provides stable teleoperation under variable delay without the need for a priori knowledge of the delay characteristics unlike the Smith predictor based techniques. In 2006, they formalized the CDOB and mathematically showed that the output of the CDOB yields undelayed position information of the slave system [44]. In 2007, they presented the stability analysis of CDOB and investigated the effects of natural angular frequency, damping coefficient and cutoff frequency of CDOB on the system performance [45]. None of these presented a transparency argument since the CDOB is a disturbance observer, therefore the net external disturbance due to environment forces and disturbance due to delay in the communication channel are inseparable from its output. This problem was addressed in the authors' more recent work [46]. The authors propose the use of "Reaction Torque Observer (RTOB)", developed by Murakami, Yu and Ohnishi [47], to estimate the external forces at the master and slave systems. The main principle behind the implementation of RTOB is the subtraction of known internal disturbances and nonlinearities from the total disturbance estimated by a Disturbance Observer (DOB) to yield the net external disturbance due to environment forces. By incorporating three different observers (CDOB, RTOB and DOB), the authors achieve stable and transparent teleoperation robust to variable delay. The 4-channel architecture is used for transparency. In 2010, Natori et al. published their latest work on their CDOB based approach to delay compensation where they meticulously detailed the mathematical model of the CDOB, DOB and RTOB and presented their results against a conventional

Smith predictor based technique [48].

1.3 Thesis Contributions and Organization

In this thesis, a delay compensation technique for stable and force reflecting bilateral teleoperation under time delay is proposed. A novel predictor observer (PROB) is developed and its stability is shown using Lyapunov analysis. A 3-channel architecture, which is a derivation from the classic 4-channel architecture is utilized for force reflection and it is explained along with the disturbance observers (DOB) and reaction torque observers (RTOB) as the components of the proposed control architecture that delivers stable and force reflecting teleoperation.

The proposed observer predicts the future states of the remote system based on a linear and nominal model of the system and these estimated states are used in the calculation of the control input for the system. Unlike the conventional bilateral control schemes in the literature, the control input for the remote system is computed at the local site and sent through the communication channel allowing both the controllers and PROB run at the same sampling rate and be robust to unexpected problems in the communication channel such as sampling and lost packets. Sampling problems with the control input do not cause significant errors in the tracking performance. In order to improve the accuracy of the PROB estimations, the nonlinearities and parametric uncertainties of the remote system are eliminated by the DOBs. DOB is also applied to the local system to render the systems identical. Operator and environment forces are estimated using RTOBs in order to eliminate the need for costly force sensors. The 3-channel architecture is realized by exchanging the control input for the remote system, the position

of the remote system and estimated environment force acting on the remote system.

Proposed delay compensation method is compared to two other techniques in the literature: P-like controller [24] and Communication Disturbance Observer [46] in a Matlab/Simulink simulation environment. Simulations are carried out for a pair of 1-DOF robot arms and 2-DOF pantograph robots to validate the proposed method. For real-time experiments, these manipulators are produced at the Sabancı University Mechatronics laboratory and experimental results are presented where the proposed method delivers stable and force reflecting teleoperation.

The contributions of the thesis can be summarized as:

- An observer based approach to delay compensation in linear and nonlinear bilateral systems is proposed. For this purpose a novel predictor observer is developed and its stability is shown by a Lyapunov analysis.

- Both the local and remote system controllers are implemented at the local site along with the predictor observer allowing them to run at their native sampling rate, robust to sampling problems in the communication channel.

- Force reflection is achieved using a modified version of the 4-channel architecture, exchanging 3 signals.

- Both linear (1-DOF robot arms) and nonlinear (2-DOF pantograph robots) are controlled in a stable and force reflecting teleoperation scheme using the proposed method. Experiments are conducted in real-time using dSpace1103 control card under artificial delay using Matlab/Simulink and real internet delay.

The thesis is organized as follows: Chapter II presents an overview of bilateral teleoperation systems. A model for bilateral teleoperation systems is presented and the control model for observer based approaches is given. The adopted observers DOB and RTOB are explained and the 4-channel architecture, basis for the proposed 3-channel architecture, is presented in this chapter as well. In Chapter III, the proposed control architecture is explained. The PROB is developed and its stability is shown using a Lyapunov analysis, the master and slave control inputs are designed in a Lyapunov framework and the position tracking performance and steady state analysis of the proposed method are investigated. The simulation results for the proposed method and two other methods are presented and analyzed in Chapter IV. Chapter V presents the experimental results on the performance of the proposed method on two different test beds and two delay conditions and their discussion. Finally, Chapter VI concludes the thesis with an overall discussion of the proposed method and its performance and discusses possible future work on the subject.

1.4 Notes

This thesis work is developed in the context of a TUBITAK (The Scientific and Technological Research Council of Turkey) and NSF (National Science Foundation) funded joint research project under the grant 106M533.

The following publications are produced from this thesis:

Journal Articles

- Delay Compensation in Force Reflecting Bilateral Teleoperation Using

Predictor Observers, D. Özçelik, T. Leblebici, S. Dikyar, M. Ünel, A. Şabanoviç, IEEE Transactions on Industrial Informatics (TII 2011). (to be submitted)

Conference Proceedings

- Delay Compensation for Nonlinear Teleoperators Using Predictor Observers, S. Dikyar, T. Leblebici, D. Özçelik, M. Ünel, A. Şabanoviç, S. Bogosyan, IEEE International Conference on Industrial Electronics, Control and Instrumentation (IECON 2010), November 7-10, Glendale, AZ, USA.

- İki Yönlü Denetim Sistemlerinde Kuvvet Tabanlı Kestirici Gözlemci ile Zaman Gecikme Telafisi, D. Özçelik, T. Leblebici, S. Dikyar, M. Ünel, A. Şabanoviç, TOK'11: Otomatik Kontrol Ulusal Toplantısı, Dokuz Eylül Üniversitesi, İzmir, Türkiye, 14-16 Eylül, 2011.

- Doğrusal Olmayan İki Yönlü Denetim Sistemlerinde Gözlemci Tabanlı Zaman Gecikme Telafisi, T. Leblebici, S. Dikyar, D. Özçelik, M. Ünel, A. Şabanoviç, TOK'10: Otomatik Kontrol Ulusal Toplantısı, Gebze Yüksek Teknoloji Enstitüsü, Kocaeli, Türkiye, 21-23 Eylül 2010.

1.5 Nomenclature

List of symbols and their descriptions used in this thesis are given in order of appearance.

Symbol	Description
x_o	Operator state
x_m	Master system state
x_s	Slave system state
F_e	Environment force
F_s	Force sensed by slave system
F_m	Force exerted on operator by master system
$\hat{x}_s$	Estimated slave state
J_s	Inertia of linear slave system
q_s	Slave position
b_s	Damping of linear slave system
τ_s	Control input for slave system
$\mathbb{J}_s$	Slave robot Jacobian
$\mathbb{J}_m$	Master robot Jacobian
J_m	Inertia of linear master system
q_m	Master position
b_m	Damping of linear master system
τ_m	Control input for master system
F_h	Human force
$D_s(q_s)$	Inertia matrix of nonlinear slave system
$C_s(q_s, \dot{q}_s)$	Coriolis-centripetal matrix of nonlinear slave system
$F_{G_s}(q_s)$	Gravitational force vector on nonlinear slave system
B_s	Damping matrix of nonlinear slave system
$D_m(q_m)$	Inertia matrix of nonlinear master system
$C_m(q_m, \dot{q}_m)$	Coriolis-centripetal matrix of nonlinear master system
$F_{G_m}(q_m)$	Gravitational force vector on nonlinear master system
B_m	Damping matrix of nonlinear master system
τ_d	External disturbance
τ_{dis}	Total disturbance
P_{nom}	Nominal transfer function
P	Actual transfer function
G	Transfer function of the low-pass filter
τ_{int}	Internal disturbance
τ_{ext}	Net external force
F	Coulomb friction
Z_t	Transmitted impedance
Z_e	Environment impedance
Z_m	Master impedance
Z_s	Slave impedance

Symbol	Description
x_e	Estimated slave state
K_p	Proportional control gain for position error
K_d	Derivative control gain for position error
K_f	Proportional control gain for force error
$\hat{F}_e$	Estimated environment force
$\hat{F}_h$	Estimated human force
$T_1(t)$	Time delay from master to slave side
$T_2(t)$	Time delay from slave to master side
$T(t)$	Roundtrip time delay in the system
$\hat{p}$	Intermediate observer variable
p_e	Estimated slave position
u_0	Observer control input
u_{0eq}	Equivalent part of observer control input
p_d	Delayed slave position
$e(t)$	Observer error
σ	Sliding surface
C	Slope of the sliding surface
V	Lyapunov function
K	Discontinuous control gain
r	Filtered error
λ	Filtered error parameter
e_f	Force error
g	Cut-off frequency of disturbance observer

Chapter II

2 Overview of Bilateral Teleoperation System

In this chapter, a bilateral teleoperation system is modeled and the control structure for an observer based approach is given. Linear and nonlinear dynamics of manipulators used in bilateral systems are shown and the two observers (Disturbance Observer and Reaction Torque Observer) used in the system are explained. The 4-channel architecture proposed by Lawrence, which serves a basis for the 3-channel architecture used in this work is also presented in this chapter.

2.1 Bilateral Teleoperation System Model

A bilateral system generally consists of five components: Operator, master (local) system, communication channel, slave (remote) system and environment. The goal of the system is to make the slave system track the master system position while reflecting the environment forces back to the operator. In the literature, proposed techniques require the exchange of position, velocity and force information between the two systems to achieve this goal. Figure 2.1 shows the block diagram for a bilateral teleoperation system model. In this model, $x_o,\ x_m,\ x_s$ are the states of the human operator,

master and slave systems respectively, F_e, F_s, F_m denote the environment force, force sensed by the slave system and force exerted on the operator by the master system respectively and T_1, T_2 are the amounts of delay in the communication channel in both directions. In a stable and transparent

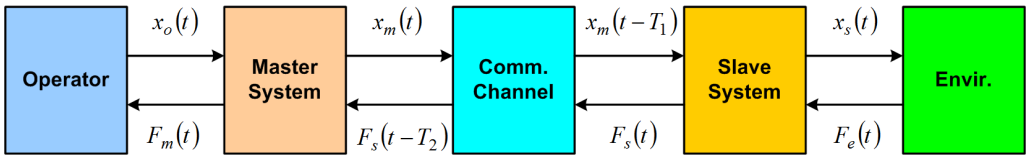

Figure 2.1: Model of a bilateral teleoperation system

teleoperation, the states of the master and slave should be equal and the environment force should be reflected to the operator. To achieve this, a delay compensation method is necessary to extract the necessary information from the delayed signals. Depending on the delay compensation technique, the exchanged signals may differ. In an observer based technique, such as the one presented in this work, the measured signals from the slave system are input to an estimation system and the control signal for the slave is computed at the local site and sent through the communication channel. Figure 2.2 shows the block diagram for an observer based bilateral teleoperation system model. Different to the previous model, the slave control signal u_s is sent to the slave side, slave state x_s is received to run the estimation system and the estimated slave state $\hat{x}_s$ is fed to the master system to run the slave controller.

2.1.1 Linear Manipulator Dynamics

Linear manipulators are often used in bilateral system modeling for their simplicity. In this section, the bilateral system is assumed to be consisting

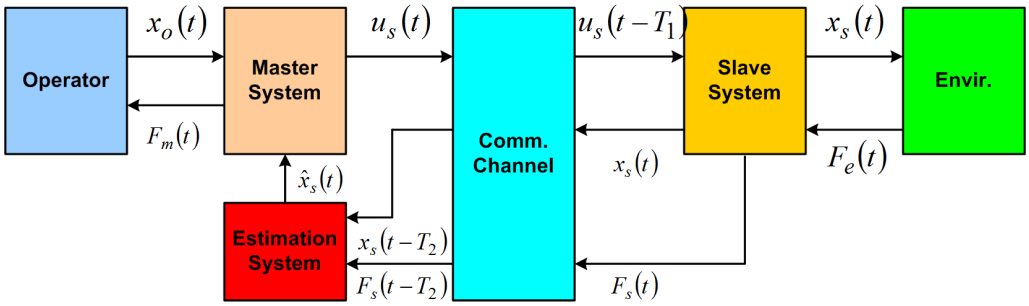

Figure 2.2: Model of an observer based bilateral teleoperation system

of two 1-DOF robot arms acting as the master and slave. The dynamical equation for the slave 1-DOF robot arm can be written as

$$J_s\ddot{q}_s(t) + b_s\dot{q}_s(t) = \tau_s(t) - \mathbb{J}_s^T F_e(t) \tag{2.1}$$

where J_s, b_s, $\ddot{q}_s$, $\dot{q}_s$, denote the moment of inertia, damping coefficient, angular acceleration and angular velocity of the robot arm, respectively. The input torque is denoted by τ_s, the Jacobian of the slave robot arm is denoted by $\mathbb{J}_s$ and environment torque acting on the slave system is denoted by F_e. The master 1-DOF robot arm which is manipulated by a human operator can be described similarly as

$$J_m\ddot{q}_m(t) + b_m\dot{q}_m(t) = \mathbb{J}_m^T F_h(t) - \tau_m(t) \tag{2.2}$$

where subscript m stands for the master robot, F_h is the operator force and τ_m is the input torque for the master robot which reflects the environment forces back to the operator.

2.1.2 Nonlinear Manipulator Dynamics

For a more complex model consisting of a pair of n-DOF nonlinear robot arms, the dynamical equation equation for the slave robot are given as

$$D_s(q_s)\ddot{q}_s + C_s(q_s, \dot{q}_s)\dot{q}_s + F_{Gs}(q_s) + B_s\dot{q}_s = \tau_s - \mathbb{J}_s^T F_e \tag{2.3}$$

where q_s is the vector of joint angles, $D_s(q_s)$ is the $n \times n$ positive-definite inertia matrix, $C_s(q_s, \dot{q}_s)$ is the $n \times n$ Coriolis-centripetal matrix, $F_{Gs}(q_s)$ is the $n \times 1$ gravitational force vector, B_s is the viscous friction (damping) matrix, $\mathbb{J}_s$ is the Jacobian matrix and F_e is the vector of environment forces acting on each joint. The input torque vector is denoted by τ_s. The master robot dynamics can be written similarly as

$$D_m(q_m)\ddot{q}_m + C_m(q_m, \dot{q}_m)\dot{q}_m + F_{Gm}(q_m) + B_m\dot{q}_m = \mathbb{J}_m^T F_h - \tau_m \tag{2.4}$$

where, as in the linear dynamical equation subscript m stands for the master robot and F_h is the vector of operator forces acting on each joint.

2.2 Disturbance Observer

Disturbance observers (DOBs) are established at both master and slave systems to linearize the dynamics and eliminate internal disturbances due to parametric uncertainties and external disturbance. This enables the control of nonlinear systems using controllers based on linear system models.

Nonlinear dynamics of an n DOF robot manipulator can be written as

$$\tau = D(q)\ddot{q} + C(q, \dot{q})\dot{q} + F_G(q) + B\dot{q} + \tau_d \tag{2.5}$$

where q is the vector of joint angles, $D(q)$ is the $n \times n$ positive-definite inertia matrix, $C(q, \dot{q})$ is the $n \times n$ Coriolis-centripetal matrix, $F_G(q)$ is the $n \times 1$ gravitational force vector, B is the viscous friction (damping) matrix, τ_d is an external disturbance vector and τ is the control input vector.

Inertia and damping matrices can be written as the sum of a nominal matrix and an unknown disturbance matrix which consists of the parametric uncertainties and disturbance:

$$D(q) = D_{nom} + \tilde{D}(q),\ B = B_{nom} + \tilde{B}$$

where the nominal inertia and damping matrices are defined as

$$D_{nom} = diag(J_{nom_1}, J_{nom_2}, \ldots, J_{nom_n}),\ B_{nom} = diag(b_{nom_1}, b_{nom_2}, \ldots, b_{nom_n})$$

Rewriting equation (2.5) in terms of nominal inertia and damping matrices implies

$$D_{nom}\ddot{q} + B_{nom}\dot{q} + \tau_{dis} = u \tag{2.6}$$

where u is the control input and τ_{dis} is the total disturbance acting on the system which is defined as

$$\tau_{dis} = \tilde{D}(q)\ddot{q} + C(q, \dot{q})\dot{q} + \tilde{B}\dot{q} + F_G(q) + \tau_d \tag{2.7}$$

In order to estimate the total disturbance at each joint, a disturbance observer [49] is integrated to each joint of the robot (see Fig. 2.3). In Figure 2.3, $P_{nom_i}(s)$ denotes the nominal transfer function of a linear system, characterized by the actual transfer function $P_i(s)$, modeling each joint (i) and $G(s) = \frac{g}{s+g}$ is the transfer function of the low-pass filter used to estimate the

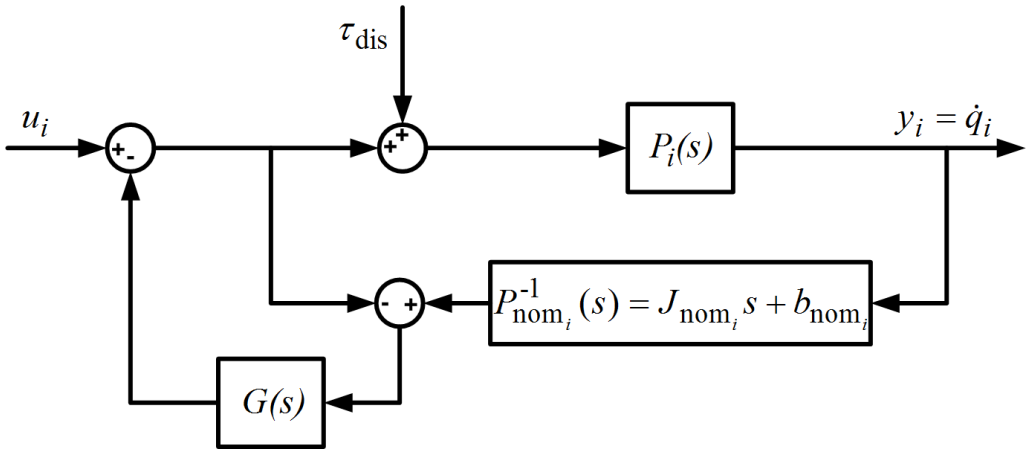

Figure 2.3: Disturbance Observer

total disturbance. By using superposition, the system output can be written [50] as

$$y_i = G_{u_i - y_i}(s) u_i + G_{\tau_{dis} - y_i}(s) \tau_{dis} \tag{2.8}$$

where

$$G_{u_i - y_i}(s) = \frac{P_i(s) P_{nom_i}(s)}{P_{nom_i}(s) + (P_i(s) - P_{nom_i}(s)) G(s)} \tag{2.9}$$

and

$$G_{\tau_{dis} - y_i}(s) = \frac{P_i(s) P_{nom_i}(s)(1 - G(s))}{P_{nom_i}(s) + (P_i(s) - P_{nom_i}(s)) G(s)} \tag{2.10}$$

If $G(s) \approx 1$, then the transfer functions given in (2.8)-(2.10) are approximated as

$$G_{u_i - y_i}(s) \approx P_{nom_i}(s) = \frac{1}{J_{nom_i} s + b_{nom_i}} \tag{2.11}$$

and

$$G_{\tau_{dis} - y_i}(s) \approx 0 \tag{2.12}$$

Equations (2.11) and (2.12) show that the total disturbance acting on the

system is eliminated in the low frequency region characterized by the filter's cut-off frequency and the input/output relationship of the system is linear with nominal parameters. As a result, the nonlinear robot dynamics given in (2.5) will be reduced to the following linear dynamics

$$J_{nom_i}\ddot{q}_i + b_{nom_i}\dot{q}_i = u_i, \quad i = 1, 2, \ldots, n \tag{2.13}$$

Notice that equation (2.13) can be used for both slave and master robots. Thus, the linear controllers can be used to control the robots.

2.3 Reaction Torque Observer

Reaction Torque Observer (RTOB) enables sensorless force estimations at master and slave systems. The total disturbance estimated by DOB includes the parametric uncertainties, system nonlinearities, friction, coupling, gravity and the net external force applied to the systems. Although not exactly known, all the terms in the total disturbance can be approximated to a degree, and subtracted from total disturbance to yield the net external force. The more precise the approximations are, the better the force estimation becomes. RTOBs are used in this work to eliminate the need for costly force sensors.

For a nonlinear system, total disturbance calculated by a DOB for each joint is given as

$$\tau_{dis} = \tau_{int} + \tau_{ext} + F_i + D_i\dot{q}_i + (J_i - J_{nom_i})\ddot{q}_i + (b_i - b_{nom_i})\dot{q}_i \tag{2.14}$$

where τ_{int} is the interactive torque, including the coupling inertia torque,

Coriolis forces, gravitation etc., τ_{ext} is the reaction torque which is nonzero when the system contacts with the environment, F_i and $D_i\dot{q}_i$ are the Coulomb and viscous friction respectively, $(J_i - J_{nom_i})\ddot{q}_i$ is the self-inertia variation torque and lastly $(b_i - b_{nom_i})\dot{q}_i$ is the torque pulsation due to the flux distribution variation of the motor. As explained in the previous section, subtracting these forces from the nonlinear system dynamics yields a linear system with nominal parameters given in equation (2.13). With a nonlinear model of the system, these terms in total disturbance can be approximated and subtracted to find the net external torque.

$$\tau_{ext} = \tau_{dis} - \tau_{int} - F_i - D_i\dot{q}_i - (J_i - J_{nom_i})\ddot{q}_i - (b_i - b_{nom_i})\dot{q}_i \tag{2.15}$$

2.4 4-Channel Architecture

Stable manipulation and transparency are the two main goals in bilateral control architecture design. Transparency requires that transmitted impedance is matched with the environment impedance ($Z_t = Z_e$) or the following conditions are satisfied:

$$x_s = x_m$$
$$F_h = -F_e$$

the slave tracks the master position precisely and the environment force is perceived by the human operator. Stable tracking can be achieved by passivity. According to the passivity theory, if the subsystems (master, slave, communication channel, environment and human) are passive, then the interconnected bilateral teleoperation system is also passive. In the literature,

two, three and four channel architectures have been proposed for stable force reflecting teleoperation. In this work, a modified version of the 4-channel architecture is used in which the master and slave positions and operator and environment forces are exchanged. In Figure 2.4 the master and slave dynamics are represented by the impedances Z_m and Z_s respectively. Similarly, C_m and C_s represent the master and slave controllers and $C_1 - C_4$ blocks denote the position and force controllers in both directions.

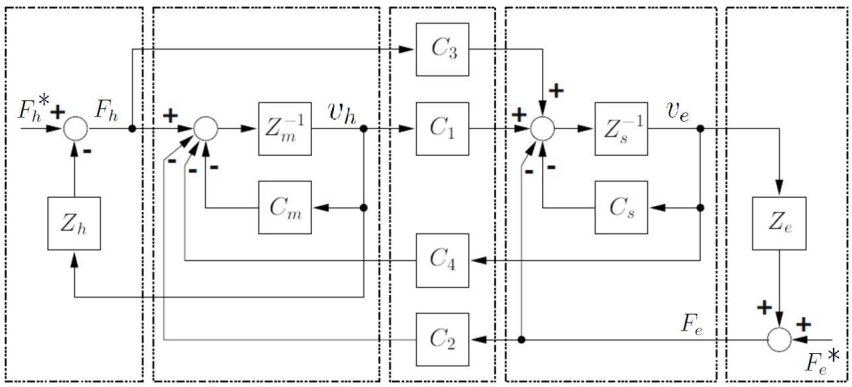

Figure 2.4: Block diagram of a four channel bilateral teleoperation system

The overall force reflecting bilateral teleoperation system can be defined using the hybrid matrix

$$\begin{bmatrix} F_h(s) \\ -V_s(s) \end{bmatrix} = \underbrace{\begin{bmatrix} h_{11}(s) & h_{12}(s) \\ h_{21}(s) & h_{22}(s) \end{bmatrix}}_{\triangleq H(s)} \begin{bmatrix} V_m \\ F_e \end{bmatrix} \tag{2.16}$$

The parameters of the hybrid matrix are calculated by solving the equation (2.16) and they are defined in terms of the subsystems of the bilateral system

designed based on 4-channel control structure as

$$
\begin{aligned}
h_{11} &= (Z_m + C_m)D(Z_s + C_s - C_3C_4) + C_4 \\
h_{12} &= -(Z_m + C_m)D(I - C_3C_2) - C_2 \\
h_{21} &= D(Z_s + C_s - C_3C_4) \\
h_{22} &= -D(I - C_3C_2)
\end{aligned}
$$

where $D = (C_1 + C_3Z_m + C_3C_m)^{-1}$. The ideal hybrid matrix that yields the perfect transparency is

$$
H_{ideal}(s) = \begin{bmatrix} 0 & 1 \\ -1 & 0 \end{bmatrix}
$$

In order to satisfy the ideal condition of the hybrid matrix, the control parameters $C_1 - C_4$ should be chosen as

$$
\begin{aligned}
C_1 &= Z_s + C_s \qquad & C_2 &= I \\
C_3 &= I & C_4 &= -(Z_m + C_m)
\end{aligned}
$$

where acceleration measurements are required to design the master and slave controllers C_m and C_s since the master and slave impedances contain 's' terms ([25],[29],[51]). A method to avoid this problems is proposed in [52] providing transparency by designing the controllers as $C_1 = C_s$, and $C_4 = -C_m$. Lawrence concludes that stability and transparency are two conflicting characteristics, and use of 4-channel architecture increases transparency while decreasing stability.

Chapter III

3 Delay Compensation in Bilateral Control Systems Using Predictor Observer (PROB)

In this chapter, the control architecture and components of an observer based approach to communication delay problem are presented. Slave controller is designed at the master side, whose feedback is generated by an observer which predicts the states of the slave. In the subsequent subsections three channel control architecture is explained, a novel predictor observer and two controllers are designed and their stability is shown in a Lyapunov framework, the position tracking performance is analyzed and the steady state analysis is given.

3.1 Proposed Control Architecture

In the proposed delay compensation scheme, control input is designed at the master side by using the future values of the slave's states estimated by a predictor observer designed in a sliding mode control framework and sent to the slave. Thus, the slave system does not require any information from master side except the control input. Therefore for the delay compensation technique that combines both the Predictor Observer (PROB) and 4-channel architecture, the fourth channel is revealed as unnecessary. Then,

the proposed control architecture becomes 3-channel architecture where control input, environment force and slave position are transmitted (Fig. 3.1). Master and slave systems are linearized and external disturbances are eliminated by the Disturbance Observer (DOB). Net external forces are estimated using Reaction Torque Observer (RTOB), eliminating the need to use costly force sensors.

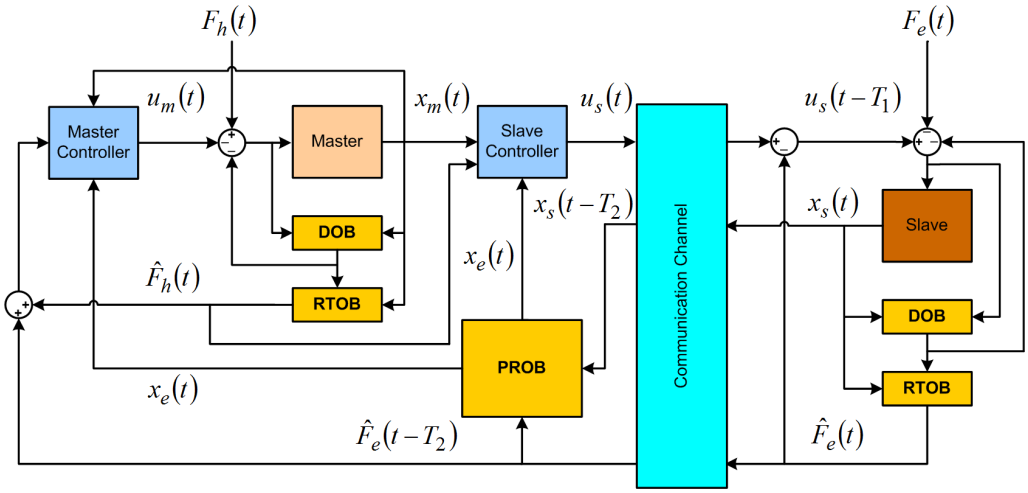

Figure 3.1: Three channel controller architecture

Acceleration control is performed on both the master and slave robots. In the master controller a Proportional-Derivative (PD) controller that pushes master's position to slave's estimated position and a Proportional force controller that defines the force error as the sum of estimated environment and human forces is used. The equation that provides control reference in acceleration dimension for master is given as

$$\ddot{x}_m(t) = K_{p_m}(x_e(t) - x_m(t)) + K_{d_m}(\dot{x}_e(t) - \dot{x}_m(t)) \\ -K_{f_m}(\hat{F}_e(t - T_2(t)) + \hat{F}_h(t)) \quad (3.1)$$

where $x_m,\ \dot{x}_m,\ \ddot{x}_m$ are the position, velocity and acceleration of the master robot, respectively. $x_e,\ \dot{x}_e$ denote the estimated slave position and velocity and $\hat{F}_e$ and $\hat{F}_h$ denote the estimated environment and human forces by Reaction Torque Observer (RTOB), respectively. $K_{p_m},\ K_{d_m},\ K_{f_m}$ are the gains for the proportional, derivative and proportional force controllers, respectively.

For the slave, a PD controller is designed at the master side to push the slave's position to master's position and is combined with the estimated human force ($\hat{F}_h(t)$). The estimated environment force ($\hat{F}_e(t)$) is not included in the control input since it is subtracted from the control input at the slave side to avoid an unnecessary delay of the signal . The acceleration controller that is designed at the master side is defined as

$$\ddot{x}_s(t) = K_{p_s}(x_m(t) - x_e(t)) + K_{d_s}(\dot{x}_m(t) - \dot{x}_e(t)) - K_{f_s}\hat{F}_h(t) \tag{3.2}$$

where the subscript s stands for the slave robot.

The use of disturbance observers at the master and slave sides eliminate all internal and external forces acting on the systems, necessitating the inclusion of force terms in the control input. In this architecture, human and environment forces are applied to the systems via the designed controllers.

3.2 Predictor Observer (PROB)

An observer that predicts the states of the slave is designed at the master side. The predictor observer is designed over a linear and nominal slave model that is obtained by disturbance observers in the master and slave sides.

The linear slave dynamics can be expressed by the following scalar differ-

ential equations in state-space

$$\begin{aligned} \dot{p}(t) &= \omega(t) \\ J_s\dot{\omega}(t) + b_s\omega(t) &= \tau_s(t) - \mathbb{J}_s^T F_e(t) \end{aligned} \tag{3.3}$$

where $\mathbb{J}_s$ is the Jacobian of the slave manipulator and $F_e(t)$ is the environment force acting on the slave.

Suppose the time delays from master to slave and from slave to master are denoted by $T_1(t)$ and $T_2(t)$, respectively. The input to the slave robot will be $\tau_s = u(t - T_1(t)) - \mathbb{J}_s^T F_e(t)$, since the environment force is estimated on the slave side and therefore will be added to the delayed control signal at the slave side. On the other hand, the position of the slave will reach to the master side as $p_d(t) = p_s(t - T_2(t))$ as depicted on Fig. 3.1.

Considering contact with environment and delay in the communication channel, the equations for the proposed observer are given as

$$\begin{aligned} \dot{\hat{p}}(t) &= \hat{\omega}(t) \\ J_s\dot{\hat{\omega}}(t) + b_s\omega_e(t) &= u_s(t) - \mathbb{J}_s^T \hat{F}_e(t - T_2(t)) + u_0(t) \end{aligned} \tag{3.4}$$

$$\begin{aligned} \dot{p}_e(t) &= \omega_e(t) \\ J_s\dot{\omega}_e(t) &= J_s\dot{\omega}_d(t) - u_{0eq}(t) \end{aligned} \tag{3.5}$$

where $\hat{p}$ and $\hat{\omega}$ are the intermediate observer variables, $p_e(t)$ and $\omega_e(t)$ are the estimated position and velocity of the slave system, $u_s(t)$ is the control input for the slave system, $\hat{F}_e(t - T_2(t))$ is the environment force estimated at the slave side by RTOB that has undergone an inevitable delay of $T_2(t)$ in the communication channel, u_0 and u_{0eq} are the observer control input and its

equivalent part respectively. For the sake of the stability analysis, we should note that the environment force ($\hat{F}_e$) is assumed to be bounded at all times ($\hat{F}_e \in \mathcal{L}_\infty$). This assumption is valid since the physical force exerted by the environment will always be a measurable quantity, and thus stay bounded.

In order to design the observer control input u_0, the observer error is defined as the difference between delayed position (p_d) and observer variable ($\hat{p}$). The error, its first and second derivatives are

$$e(t) = p_d(t) - \hat{p}(t),\ \dot{e}(t) = \omega_d(t) - \hat{\omega}(t),\ \ddot{e}(t) = \dot{\omega}_d(t) - \dot{\hat{\omega}}(t) \tag{3.6}$$

If the value of $\dot{\hat{\omega}}(t)$ is substituted from equation (3.4) into the second derivative of the observer error

$$\ddot{e}(t) = \dot{\omega}_d(t) + \frac{1}{J_s}(b_s\omega_e(t) - u_s(t) - u_0(t) + \mathbb{J}_s^T\hat{F}_e(t - T_2(t))) \tag{3.7}$$

is obtained. In order to achieve finite time convergence of the observer error to 0, observer input u_0 is designed using Sliding Mode Control (SMC) theory, therefore a sliding surface σ is defined as

$$\sigma = \dot{e}(t) + Ce(t) \tag{3.8}$$

where C is the slope of the sliding surface. If the first derivative of the sliding surface is taken and the value of second derivative of the error from equation (3.7) is substituted

$$\dot{\sigma} = \dot{\omega}_d(t) + \frac{1}{J_s}(b_s\omega_e(t) - u_s(t) - u_0(t) + \mathbb{J}_s^T\hat{F}_e(t - T_2(t))) + C\dot{e}(t) \tag{3.9}$$

is obtained. The equivalent control value can be calculated by setting $\dot{\sigma} = 0$ since this condition implies that $\sigma = 0$ and is not changing. Then, u_{0eq} becomes:

$$u_{0eq}(t) = J_s\dot{\omega}_d(t) + b_s\omega_e(t) - u_s(t) + \mathbb{J}_s^T\hat{F}_e(t - T_2(t)) + J_sC\dot{e}(t) \tag{3.10}$$

If both sides of the equation (3.9) are multiplied by J_s, and equation (3.10) is used,

$$\begin{aligned} J_s\dot{\sigma} &= J_s\dot{\omega}_d(t) + b_s\omega_e(t) - u_s(t) + \mathbb{J}_s^T\hat{F}_e(t - T_2(t)) + J_sC\dot{e}(t) - u_0(t) \\ &= u_{0eq}(t) - u_0(t) \end{aligned} \tag{3.11}$$

is obtained. A positive definite Lyapunov function, and its first derivative are defined as:

$$V = \frac{1}{2}J_s\sigma^2 \geq 0 \Rightarrow \dot{V} = \sigma J_s\dot{\sigma} \tag{3.12}$$

If the value of $J_s\dot{\sigma}$ is substituted from equation (3.11), $\dot{V}$ can be rewritten as:

$$\dot{V} = \sigma(u_{0eq}(t) - u_0(t)) \tag{3.13}$$

If a discontinuous function $u_{0eq} - u_0 = -Ksgn(\sigma)$ is defined where $K > 0$, and the fact that $xsgn(x) = |x|$ is considered, $\dot{V}$ reduces to:

$$\dot{V} = \sigma(u_{0eq}(t) - u_0(t)) = -K\sigma sgn(\sigma) = -K|\sigma| < 0 \tag{3.14}$$

which is a negative definite function.

We should note that $K > 0$ is the gain parameter of discontinuous control and $sgn(.)$ is the well known signum function. Since the Lyapunov function

$V(t)$ is positive definite and decreasing ($\dot{V(t)} < 0$), we can conclude that $V(t)$ is bounded ($V(t) \in \mathcal{L}_\infty$). Therefore, from equation (3.12), σ^2 and σ are bounded ($\sigma \in \mathcal{L}_\infty$). From equation (3.8), it can be seen that $e(t)$ and $\dot{e}(t)$ are bounded ($e(t), \dot{e}(t) \in \mathcal{L}_\infty$). Since the sliding surface ($\sigma = 0$) will be reached in finite time ($0 \leq \tau_r < \infty$) [53], for $t \geq \tau_r$, equation (3.8) becomes:

$$\dot{e}(t) + Ce(t) = 0 \tag{3.15}$$

and it can be concluded that the observer error and its first derivative converge to zero.

$$\lim_{t \to \infty} e(t), \dot{e}(t) = 0$$

Since equation (3.8) is linear and C is constant, this convergence is exponential. If the equivalent control value is substituted into equation (3.5)

$$J_s \dot{\omega}_e(t) = -b_s \omega_e(t) + u_s(t) - \mathbb{J}_s^T \hat{F}_e(t - T_2(t)) - J_s C \dot{e}(t) \tag{3.16}$$

is obtained. It has been shown that $\dot{e}(t) \in \mathcal{L}_\infty$ and assumed that $\hat{F}_e(t - T_2(t)) \in \mathcal{L}_\infty$, therefore it is needed to show that $\omega_e(t)$ and $u_s(t)$ are also bounded in order to conclude that the observer is stable.

3.3 Design of Master Control Input

In this section a Lyapunov based controller for the master system is designed. First, the position tracking error is defined as the difference between estimated position of slave (p_e) from the predictor observer and position of the master (p_m), and the first and second derivatives of the error are given

as

$$e_m(t) = p_e(t) - p_m(t),\ \dot{e}_m(t) = \omega_e(t) - \omega_m(t),\ \ddot{e}_m(t) = \dot{\omega}_e(t) - \dot{\omega}_m(t) \quad (3.17)$$

As a preliminary to the Lyapunov function, a filtered error r_m is defined as:

$$r_m = \dot{e}_m(t) + \lambda_m e_m(t) \quad (3.18)$$

where $\lambda_m > 0$ is a design parameter. Using the filtered error, a positive definite Lyapunov function is defined. Its first derivative is taken, the derivative of r_m is computed from equation (3.17) and the value of $\ddot{e}$ is substituted from (3.18):

$$\begin{aligned} V &= \frac{1}{2} J_m r_m^2 \geq 0 \Rightarrow \dot{V} = J_m r_m \dot{r}_m \\ &= r_m J_m(\ddot{e}_m + \lambda_m \dot{e}_m) = r_m(J_m \dot{\omega}_e(t) - J_m \dot{\omega}_m(t) + \lambda_m J_m \dot{e}_m) \end{aligned} \quad (3.19)$$

Nominal master dynamics are given as $J_m\ddot{\Theta}_m + b_m\dot{\Theta}_m = \tau_m$. If this expression is substituted into equation (3.19)

$$\dot{V} = r_m(J_m \dot{\omega}_e(t) + b_m \omega_m(t) - \tau_m(t) + \lambda_m J_m \dot{e}_m) \quad (3.20)$$

is obtained. If $\omega_m(t) = \omega_e(t) - \dot{e}_m(t)$ is further substituted into equation (3.20), $\dot{V}$ can be rewritten as:

$$\dot{V} = r_m\left(J_m \dot{\omega}_e(t) + b_m \omega_e(t) - \tau_m(t) + (\lambda_m J_m - b_m)\dot{e}_m\right) \quad (3.21)$$

In order to achieve force reflecting bilateral operation, the force error is defined as $e_f = F_h + F_e$. Since the external forces are estimated by the RTOBs,

they are denoted as $\hat{F}_h$ and $\hat{F}_e$. Since the environment force estimation reaches the master side with a delay of $T_2(t)$, the force error is written as:

$$e_f(t) = \hat{F}_h(t) + \hat{F}_e(t - T_2(t))$$

Similar to the previous assumption, it is assumed that the estimated human force will always be bounded ($\hat{F}_h(t) \in \mathcal{L}_\infty$) since a human operator will always exert a finite amount of force on the master system. Using these two assumptions, it can be concluded that the force error will always be bounded ($e_f \in \mathcal{L}_\infty$).

In light of equation (3.21), the master control input is designed to be

$$\tau_m(t) = u_m(t) = J_m\dot{\omega}_e(t) + b_m\omega_e + (\lambda_m J_m - b_m)\dot{e}_m + k_m r_m - K_{f_m} e_f \quad (3.22)$$

where $k_m,\ K_f > 0$ are control gain parameters. If the control input from equation (3.22) is substituted into equation (3.21), the derivative of the Lyapunov function becomes

$$\dot{V} = -k_m r_m^2 + K_{f_m} r_m e_f \quad (3.23)$$

The control gain k_m can be written as the sum of products of different positive gains ($k_m = k_{1m} + k_{2m}K_{f_m}^2$). Then equation (3.23) becomes

$$\dot{V} = -k_{1m} r_m^2 + K_{f_m} r_m e_f - k_{2m} K_{f_m}^2 r_m^2 \quad (3.24)$$

Utilizing the nonlinear damping property (see Appendix A), the last two

terms in equation (3.24) can be rewritten as

$$K_{f_m} r_m e_f - k_{2m} K_{f_m}^2 r_m^2 \leq \frac{e_f^2}{k_{2m}} \tag{3.25}$$

then equation (3.24) can be rewritten as

$$\dot{V} = -k_{1m} r_m^2 + K_{f_m} r_m e_f - k_{2m} K_{f_m}^2 r_m^2 \leq -k_{1m} r_m^2 + \frac{e_f^2}{k_{2m}} \tag{3.26}$$

In light of equation (3.19), the inequality (3.26) can be rewritten as

$$\begin{aligned} V = \frac{1}{2} J_m r_m^2 \Rightarrow r_m^2 = \frac{2V}{J_m} \\ \Rightarrow \dot{V} \leq -\underbrace{\frac{2k_{1m}}{J_m}}_{\equiv \beta_m} V + \underbrace{\frac{e_f^2}{k_{2m}}}_{\equiv \varepsilon_m} \Rightarrow \dot{V} \leq -\beta_m V + \varepsilon_m \end{aligned} \tag{3.27}$$

Since $e_f \in \mathcal{L}_\infty$, it can be concluded from that $\varepsilon_m \in \mathcal{L}_\infty$. The solution to the inequality (3.27) is

$$\dot{V} \leq -\beta_m V + \varepsilon_m \Rightarrow V(t) \leq V(0) exp(-\beta_m t) + \frac{\varepsilon_m}{\beta_m}(1 - exp(-\beta_m t)) \tag{3.28}$$

In light of equations (3.19), (3.27) and (3.28) it is concluded that

$$\frac{1}{2} J_m r_m^2(t) \leq \frac{1}{2} J_m r_m^2(0) exp(-\beta_m t) + \frac{J_m \varepsilon_m}{2k_{1m}}(1 - exp(-\beta_m t)) \tag{3.29}$$

Simplifying the inequality and using the property $\varepsilon_m \leq \|\varepsilon_m\|_\infty$, the following expression for r_m is obtained

$$r_m^2(t) \leq r_m^2(0) exp(-\beta_m t) + \frac{\|\varepsilon_m\|_\infty}{k_{1m}} - \frac{\|\varepsilon_m\|_\infty}{k_{1m}} exp(-\beta_m t)$$

Since the last term of this expression is always negative, the inequality can be reduced to

$$r_m^2(t) \leq r_m^2(0)exp(-\beta_m t) + \frac{\|\varepsilon_m\|_\infty}{k_{1m}} \tag{3.30}$$

which implies that r_m^2, thus r_m is ultimately bounded ($r_m \in \mathcal{L}_\infty$). Using equation (3.18) and the fact that r_m is bounded, it can be concluded that $e_m(t)$ and $\dot{e}_m(t)$ are bounded ($e_m(t), \dot{e}_m(t) \in \mathcal{L}_\infty$). Since the master is controlled by the operator, it can be assumed that the master position and its derivatives are bounded ($p_m, \omega_m, \dot{\omega}_m \in \mathcal{L}_\infty$), thus we can conclude that the estimated position and its derivatives are bounded ($p_e, \omega_e, \dot{\omega}_e \in \mathcal{L}_\infty$).

It has been shown that all the signals on the right side of the equation (3.22) are bounded. Thus the control input u_m is bounded at all times ($u_m \in \mathcal{L}_\infty$). The first two terms on the right side of equation (3.22) represent a model based feedforward controller and the third and fourth terms represent a PD controller.

3.4 Design of Slave Control Input

In this section a Lyapunov based controller for the slave system is designed. This is the last term ($u_s(t)$) in equation (3.16) that is to be shown to be bounded. Similar to the master controller, the position tracking error and its derivatives are defined as

$$e_s(t) = p_m(t) - p_e(t),\ \dot{e}_s(t) = \omega_m(t) - \omega_e(t),\ \ddot{e}_s(t) = \dot{\omega}_m(t) - \dot{\omega}_e(t) \tag{3.31}$$

We should note that these errors are simply the negative of the errors defined in the previous section. It was previously shown that $e_m(t), \dot{e}_m(t), \ddot{e}_m(t) \in \mathcal{L}_\infty$, therefore it follows that $e_s(t), \dot{e}_s(t), \ddot{e}_s(t) \in \mathcal{L}_\infty$. The control input will

be designed in a Lyapunov framework, thus a filtered error is defined as a preliminary to the Lyapunov function

$$r_s = \dot{e}_s(t) + \lambda_s e_s(t) \tag{3.32}$$

where λ_s is a design parameter. Using the filtered error r_s, a positive definite Lyapunov function and find its first derivative are defined as:

$$V = \frac{1}{2} J_s r_s^2 \geq 0 \Rightarrow \dot{V} = J_s r_s \dot{r}_s = r_s J_s(\ddot{e}_s + \lambda_s \dot{e}_s) \tag{3.33}$$

$$\dot{V} = r_s J_s(\dot{\omega}_m(t) - \dot{\omega}_e(t) + \lambda_s \dot{e}_s) = r_s(J_s\dot{\omega}_m(t) - J_s\dot{\omega}_e(t) + J_s\lambda_s\dot{e}_s) \tag{3.34}$$

Using equation (3.16), equation (3.33) can be rewritten as:

$$\dot{V} = r_s(J_s\dot{\omega}_m(t) + b_s\omega_e - u_s(t) + \mathbb{J}_s^T \hat{F}_e(t - T_2(t)) + J_s(C\dot{e} + \lambda_s\dot{e}_s)) \tag{3.35}$$

Then the control input u_s can be designed in light of equation (3.35) as

$$\begin{aligned} u_s(t) = {} & J_s\dot{\omega}_m(t) + b_s\omega_e + \mathbb{J}_s^T \hat{F}_e(t - T_2(t)) + CJ_s\dot{e} + (\lambda_s J_s - b_s)\dot{e}_s \\ & + k_s r_s - K_{f_s}\hat{F}_h(t) \end{aligned} \tag{3.36}$$

where $k_s,\ K_f > 0$ are control gain parameters. When the control input in equation (3.36) is substituted into equation (3.35)

$$\dot{V} = -k_s r_s^2 + K_{f_s} r_s \hat{F}_h(t) \tag{3.37}$$

is obtained. Similar to the previous section, the control gain k_s can be written as sum of products of different gains ($k_s = k_{1s} + k_{2s}K_{f_s}^2$), and substituted

into equation (3.37)

$$\dot{V} = -k_{1s} r_s^2 + K_{f_s} r_s \hat{F}_h(t) - k_{2s} K_{f_s}^2 r_s^2 \tag{3.38}$$

Using the nonlinear damping property, the last two terms in equation (3.38) can be written as

$$K_{f_s} r_s \hat{F}_h - k_{2s} K_{f_s}^2 r_s^2 \leq \frac{\hat{F}_h^2}{k_{2s}} \tag{3.39}$$

which leads to this inequality for $\dot{V}$:

$$\dot{V} = -k_{1s} r_s^2 + K_{f_s} r_s \hat{F}_h(t) - k_{2s} K_{f_s}^2 r_s^2 \leq -k_{1s} r_s^2 + \frac{\hat{F}_h^2}{k_2 s} \tag{3.40}$$

Using equation (3.19), inequality (3.40) can be rewritten as

$$V = \frac{1}{2} J_s r_s^2 \Rightarrow r_s^2 = \frac{2V}{J_s} \Rightarrow \dot{V} \leq -\underbrace{\frac{2k_{1s}}{J_s}}_{\equiv \beta_s} V + \underbrace{\frac{\hat{F}_h^2}{k_{2s}}}_{\equiv \varepsilon_s} \Rightarrow \dot{V} \leq -\beta_s V + \varepsilon_s \tag{3.41}$$

Since the human force estimated by RTOB is bounded ($\hat{F}_h \in \mathcal{L}_\infty$), ε_s is bounded ($\varepsilon_s \in \mathcal{L}_\infty$). The solution to the inequality (3.41) is

$$\dot{V} \leq -\beta_s V + \varepsilon_s \Rightarrow V(t) \leq V(0) exp(-\beta_s t) + \frac{\varepsilon_s}{\beta_s}(1 - exp(-\beta_s t)) \tag{3.42}$$

Using equations (3.19), (3.41) and (3.42), it can be concluded that

$$\frac{1}{2} J_s r_s^2(t) \leq \frac{1}{2} J_s r_s^2(0) exp(-\beta_s t) + \frac{J_s \varepsilon_s}{2k_{1s}}(1 - exp(-\beta_s t)) \tag{3.43}$$

Simplifying the inequality and using the property $\varepsilon_s(t) \leq \|\varepsilon_s\|_\infty$, the following expression for r_s is obtained

$$r_s^2(t) \leq r_s^2(0)exp(-\beta_s t) + \frac{\|\varepsilon_s\|_\infty}{k_{1s}} - \frac{\|\varepsilon_s\|_\infty}{k_{1s}}exp(-\beta_s t) \tag{3.44}$$

Since the last term of this expression is always negative, the inequality can be reduced to

$$r_s^2(t) \leq r_s^2(0)exp(-\beta_s t) + \frac{\|\varepsilon_s\|_\infty}{k_{1s}} \tag{3.45}$$

which implies that the position tracking error is bounded from above and can be reduced by increasing the controller gain k_{1s}. Notice that equation (3.45) is equivalent to equation (3.30), thus the boundedness arguments in the previous section follow. Since all the signals on the right side of equation (3.36) are bounded, control input u_s is bounded ($u_s \in \mathcal{L}_\infty$). At this point the boundedness of all the signals on the right side of equation (3.16) has been shown, thus $\omega_e,\ \dot{\omega}_e \in \mathcal{L}_\infty$.

3.5 Position Tracking Performance and Steady State Analysis

In order to analyze the position tracking performance of the controller, it needs to be shown that the predictor observer estimates the future states of the slave system. Initially, the delayed dynamics of the slave are written

$$\begin{aligned} \dot{p}_d(t) &= \omega_d(t) \\ J_s\dot{\omega}_d(t) + b_s\omega_d(t) &= u_s(t - T_1(t) - T_2(t)) - \mathbb{J}_s^T\hat{F}_e(t - T_2(t)) \end{aligned} \tag{3.46}$$

where $T_1(t)$ and $T_2(t)$ denote the time delays from master to slave and slave to master respectively and $T(t)$ is defined as the roundtrip delay $T_1(t) + T_2(t)$. Delayed velocity ω_d denotes the velocity of the slave delayed by $T_2(t)$ ($\omega_d(t) = \omega(t - T_2(t))$), similarly delayed acceleration $\dot{\omega}_d$ denotes the acceleration of the slave delayed by $T_2(t)$ ($\dot{\omega}_d(t) = \dot{\omega}(t - T_2(t))$ and slave control input u_s is delayed by the roundtrip delay $T(t)$ ($u_s(t - T_1(t) - T_2(t)) = u_s(t - T(t))$). If t is substituted with $t + T$ in equation (3.46)

$$J_s\dot{\omega}_d(t+T) + b_s\omega_d(t+T) = u_s(t) - \mathbb{J}_s^T\hat{F}_e(t+T_1(t)) \tag{3.47}$$

is obtained. Subtracting equations (3.16) and (3.47) yields

$$\begin{aligned} &J_s(\dot{\omega}_e(t) - \dot{\omega}_d(t+T) + b_s(\omega_e(t) - \omega_d(t+T))) \\ &\qquad = -J_sC\dot{e}(t) + \mathbb{J}_s^T(\hat{F}_e(t+T_1(t)) - \hat{F}_e(t-T_2(t))) \end{aligned} \tag{3.48}$$

Defining $\tilde{\omega}$ as the difference between estimated velocity ω_e and the future of delayed velocity ω_d by an amount equal to the round-trip delay T ($\tilde{\omega}(t) = \omega_e(t) - \omega_d(t+T)$) and substituting it into the equation (3.48) gives

$$J_s\dot{\tilde{\omega}}(t) + b_s\tilde{\omega}(t) = -J_sC\dot{e}(t) + \mathbb{J}_s^T(\hat{F}_e(t+T_1(t)) - \hat{F}_e(t-T_2(t))) \tag{3.49}$$

It was previously shown that $e, \dot{e} \in \mathcal{L}_\infty$, and the forces estimated by RTOB are bounded ($\hat{F}_e(t+T_1(t)), \hat{F}_e(t-T_2(t)) \in \mathcal{L}_\infty$). Since all the signals on the right side of equation (3.49) are bounded, it can be concluded that $\tilde{\omega}_e(t), \dot{\tilde{\omega}}(t) \in \mathcal{L}_\infty$. Similarly, $\omega_e(t), \dot{\omega}_e(t) \in \mathcal{L}_\infty$ implies that $\omega_d(t+T(t)), \dot{\omega}_d(t+$

$T(t)) \in \mathcal{L}_\infty$. Since $\omega_d(t) = \omega(t - T_2(t))$, it can be rewritten as

$$\omega_d(t + T(t)) = \omega(t + T(t) - T_2(t)) = \omega(t + T_1(t)) \tag{3.50}$$

which implies that the slave velocity and acceleration is bounded at all times $(\omega(t + T_1(t)), \dot{\omega}(t + T_1(t)) \in \mathcal{L}_\infty)$. Since all the signals in equation (3.49) are bounded, a steady state analysis can easily be made. Since the observer error converges to 0 in steady state, and

$$\lim_{t\to\infty} \hat{F}_e(t + T_1(t)) = \lim_{t\to\infty} \hat{F}_e(t - T_2(t))$$

it can be concluded that $\tilde{\omega}(t)$ and $\dot{\tilde{\omega}}(t)$ will also converge to 0.

$$\lim_{t\to\infty} \tilde{\omega}(t), \dot{\tilde{\omega}}(t) = 0 \tag{3.51}$$

Since equation (3.49) is linear and has constant coefficients, this convergence will be in exponential time and the rate of convergence will depend on b_s/J_s parameter. From definition of $\tilde{\omega}(t)$, it can be inferred that $\tilde{\omega}(t) = \omega_e(t) - \omega_d(t + T(t)) = \omega_e(t) - \omega(t + T_1(t))$, since the round-trip delay $T(t) = T_1(t) + T_2(t)$ and $\omega_d = \omega(t - T_2(t))$. Thus

$$\lim_{t\to\infty} \omega_e(t) = \lim_{t\to\infty} \omega_d(t + T(t)) = \lim_{t\to\infty} \omega(t + T_1(t)) \tag{3.52}$$

$$\lim_{t\to\infty} \dot{\omega}_e(t) = \lim_{t\to\infty} \dot{\omega}_d(t + T(t)) = \lim_{t\to\infty} \dot{\omega}(t + T_1(t)) \tag{3.53}$$

It is shown that the estimated velocity and acceleration converge to the future states of the slave. It was shown that the first term in equation (3.10) is bounded $(\dot{\omega}_d(t + T(t)) \in \mathcal{L}_\infty)$. The rest of the terms were also shown to

be bounded, thus the equivalent control signal is bounded ($u_{0eq}(t) \in \mathcal{L}_\infty$). Since the observer control input $u_0(t) = u_{0eq}(t) + Ksgn(\sigma)$ is the sum of a bounded signal and a discontinuous constant term, it is also bounded at all times ($u_0(t) \in \mathcal{L}_\infty$).

The convergence shown in equation (3.52) is in terms of velocities. In order to investigate the relationship between positions, the expression $\tilde{\omega}(t) = \omega_e(t) - \omega(t + T_1(t))$ needs to be integrated.

$$\begin{aligned}
&\int_0^t \omega_e(\tau)\,\mathrm{d}\tau - \int_0^t \omega(\tau + T_1(\tau))\,\mathrm{d}\tau = \int_0^t \tilde{\omega}(\tau)\,\mathrm{d}\tau \\
&\Rightarrow p_e(t) - p_e(0) - (p(t + T_1(t)) - p(T_1(0))) = \int_0^t \tilde{\omega}(\tau)\,\mathrm{d}\tau \\
&\Rightarrow p_e(t) - p(t + T_1(t)) = \int_0^t \tilde{\omega}(\tau)\,\mathrm{d}\tau + \underbrace{p_e(0) - p(T_1(0))}_{\varepsilon_1} \\
&= \int_0^t \tilde{\omega}(\tau)\,\mathrm{d}\tau + \varepsilon_1
\end{aligned} \tag{3.54}$$

As it can be seen from equation (3.54), the difference between the initial conditions of the observer and slave is represented by a constant ε_1. Since $\tilde{\omega}(t)$ is bounded, the integral $\int \tilde{\omega}(\tau)\,\mathrm{d}\tau$ is bounded at all times. This indicates that $p_e(t) - p(t + T_1(t))$ is bounded at all times ($p_e(t) - p(t + T_1(t)) \in \mathcal{L}_\infty$). We have previously shown that $p_e \in \mathcal{L}_\infty$, therefore $p(t + T_1(t)) \in \mathcal{L}_\infty$, the slave is position is bounded at all times.

If equation (3.54) is analyzed at $t \to \infty$

$$\lim_{t\to\infty}(p_e(t) - p(t + T_1(t))) = \underbrace{\lim_{t\to\infty}\int_0^t \tilde{\omega}(\tau)\,\mathrm{d}\tau}_{\equiv\varepsilon_2} + \varepsilon_1$$
$$= \varepsilon_2 + \varepsilon_1 = \varepsilon \tag{3.55}$$

In light of equations (3.32) and (3.45) it can be concluded that the difference between estimated position and master position is ultimately bounded

$$|\lim_{t\to\infty}(p_e(t) - p_m(t))| \leq \frac{\|\varepsilon_s\|_\infty}{k_{1s}} \tag{3.56}$$

The following can be deduced from equations (3.55) and (3.56)

$$\begin{aligned}
&|\lim_{t\to\infty}(p_m(t) - p(t + T_1(t)))| \\
&= |\lim_{t\to\infty}(p_m(t) - p_e(t) + p_e(t) - p(t + T_1(t)))| \\
&\leq |\lim_{t\to\infty}(p_m(t) - p_e(t))| + |\lim_{t\to\infty}(p_e(t) - p(t + T_1(t)))| \\
&= \frac{\|\varepsilon_s\|_\infty}{k_{1s}} + |\varepsilon|
\end{aligned} \tag{3.57}$$

Equation (3.57) shows that position tracking error is ultimately bounded.

The estimation performance of the predictor observer in simulations can be seen in Figure 3.2. Estimated position line is exactly on top of the master position, and approximately 0.5 *sec* ahead of the slave position, supporting the conclusion that the observer predicts the future states of the slave. Force estimation performance with RTOB is shown in Figure 3.3. The human force is estimated with an error of approximately 0.1 N. This error is due to the parametric uncertainties introduced to the simulations.

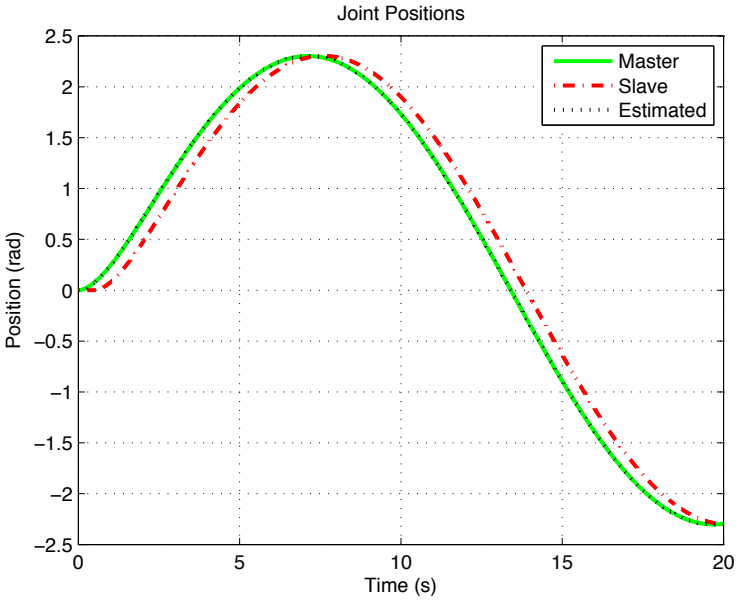

Figure 3.2: Master, slave and estimated slave positions

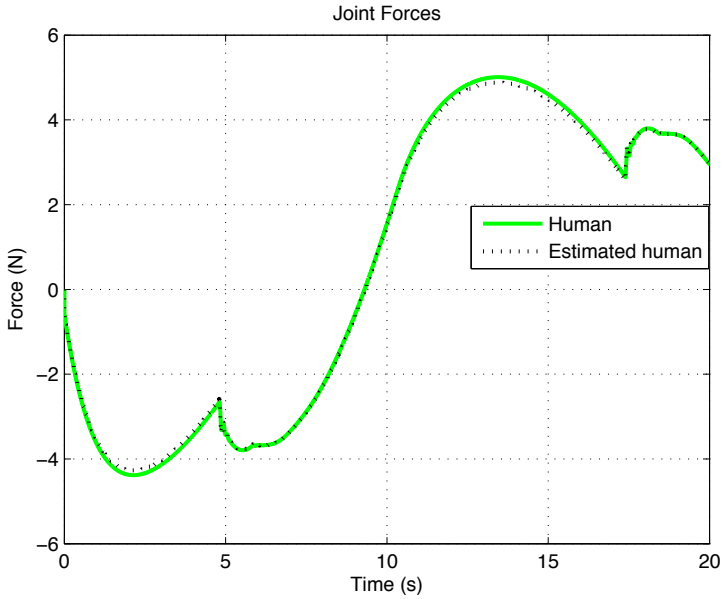

Figure 3.3: Human and estimated human forces

Chapter IV

4 Simulation Results and Discussions

In order to test the proposed control architecture and delay compensation method and compare it to two other techniques in the literature, simulations for 1-DOF robot arms and 2-DOF pantograph robots are carried out in the Matlab/Simulink environment. The two other methods are Natori and Ohnishi's "Communication Disturbance Observer" [46] and the P-like controller of Nuno, Ortega et al [24]. The simulations are executed under variable delay and for free motion and environment contact cases.

4.1 1-DOF Robot Arm Simulations

The manipulators are modeled as two 1-DOF robot arm with uniform rectangular prism rods as the arm. The nominal values of the moment of inertia of the rod and motor constants used in the simulations are given in Table 4.1. A parametric uncertainty of 10% is added to the nominal parameters during simulations.

4.1.1 P-like Controller Simulations

The simple P-like controller consists of a proportional control gain on the position error of the two systems and a damping gain on the velocity of the controlled system. There is not an explicit delay compensation method, the

Table 4.1: 1-DOF Robot Arm Parameters

	Value	Unit
Moment of Inertia of Rod (I_z)	0.00667	kgm^2
Rotor Inertia (J)	167	gcm^2
Torque Constant (Kt)	1	Nm/A
Damping Constant (B)	300	gcm^2

delayed signals are used in the control. The equations for master and slave control input are given as

$$\tau_m(t) = K_m(x_s(t - T_2) - x_m(t)) - B_m\dot{x}_m(t) \tag{4.1}$$

$$\tau_s(t) = K_s(x_m(t - T_1) - x_s(t)) - B_s\dot{x}_s(t) \tag{4.2}$$

where τ_m is the master control input, $x_m,\ x_s,\ \dot{x}_m$ are the master and slave positions and master velocity respectively and $K_m,\ B_m$ are the proportional and damping terms. The subscript s stands for the slave robot and $T_1,\ T_2$ are the amount of delay in both directions. The method requires a simple inequality to be satisfied for the four gains:

$$4B_mB_s > ({}^*T_1^2 +^* T_2^2)K_mK_s \tag{4.3}$$

where ${}^*T_1,\ {}^*T_2$ are the upper bounds on the delay in both directions. The gain values that the authors experimented with are asymmetric since the two manipulators they use are a PHANTOM Desktop and a 6-DOF TX-90 Staubli robot. Since identical 1-DOF manipulators are used in the simulations, the gains were recalculated for the purpose of these simulations. The variable delay is characterized as a normally distributed random variable

with a mean of 0.4 *sec* and standard deviation of 0.05 *sec*, and an upper bound of 0.6 *sec* is chosen to be appropriate for the delay. Then, the gains are chosen as

$$K_m = K_s = 10$$
$$B_m = B_s = 4.5$$

satisfying the inequality

$$4(4.5)^2 > (0.6^2 + 0.6^2)100 \Rightarrow 81 > 72$$

The results for the free motion simulation are presented in Figure 4.1 The

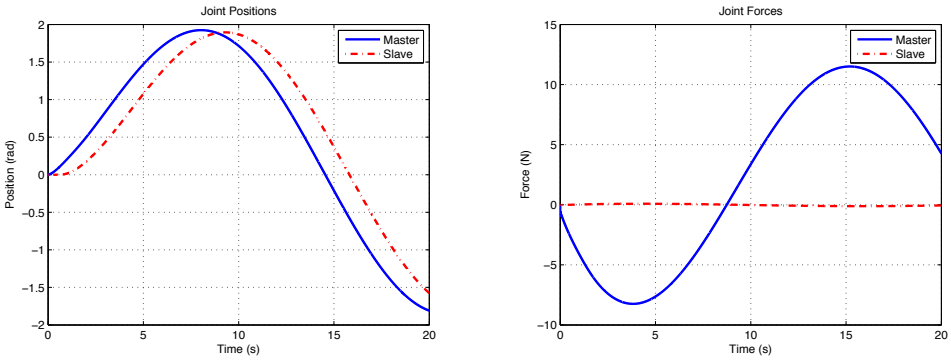

Figure 4.1: 1-DOF P-like controller free motion simulation

slave tracks the master successfully, with an error of less than 0.1 *rad*. For the contact experiment, two stiff walls are modeled at $p = \pi/2$ and $p = -\pi/2$. The results for the contact simulation are shown in Figure 4.2. The slave tracks the master until it contacts the wall and stays stationary until master leaves the obstructed zone. Then it continues tracking normally. Notice that during contact, the environment force initially oscillates to a large value

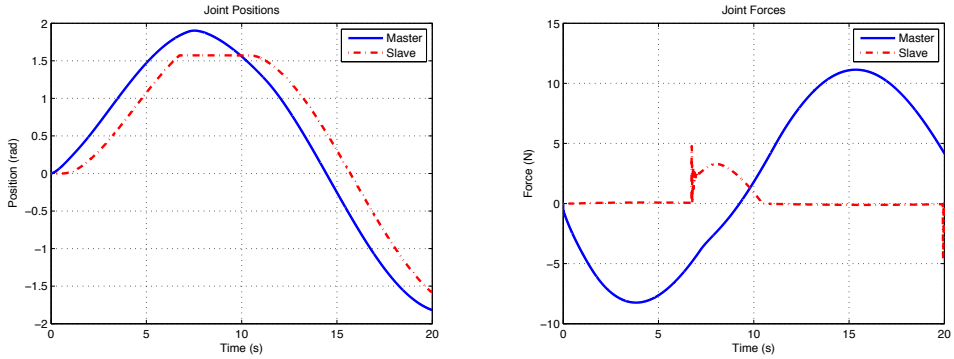

Figure 4.2: 1-DOF P-like controller contact simulation

and then becomes a smooth signal. The reason for this oscillation is the model of the wall used in the simulation. The stiff wall is modeled as a spring with a relatively large spring constant of $K = 1500\ N/m$, the slave inevitably penetrates the wall during the first milliseconds of contact and results in a large impulse reaction from the spring. Then the environment force balances the input torque and keeps the slave manipulator stationary. Since the method does not include any force terms, it is not transparent. This can be observed both in the master position and operator force, as neither respond to the environment force during the slave contacts the obstacle.

4.1.2 CDOB Simulations

Similar to the method proposed in this work, Natori and Ohnishi's method [46] depends on three observers: Communication Disturbance Observer, Disturbance Observer and Reaction Torque Observer. As explained in Section 1, CDOB estimates undelayed slave states using delayed signals. Figure 4.3 presents the block diagram of the CDOB architecture. The other two observers were explained in Section 2.2 and 2.3. There are three control gains

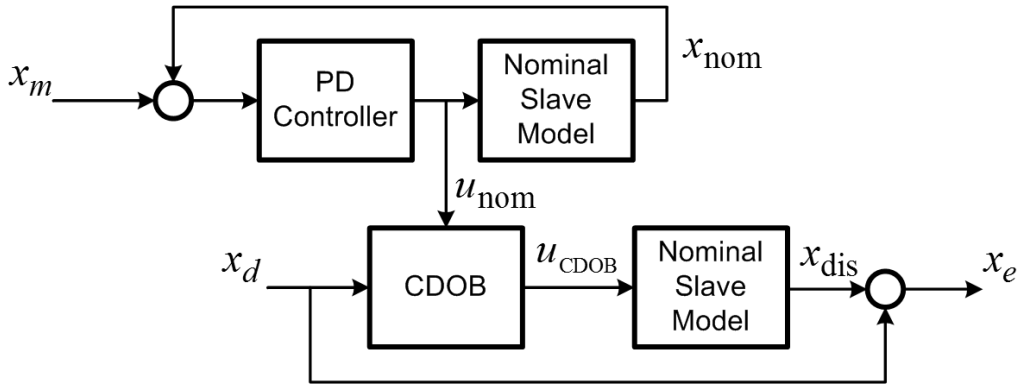

Figure 4.3: Block diagram of CDOB architecture

for each controller in the CDOB method: A Proportional-Derivative control on the position error of the two systems ($K_p,\ K_d$) and a proportional gain on the force error of the two systems (K_f). The acceleration control input for the master and slave systems are given as

$$\ddot{x}_m(t) = K_{p_m}(x_e(t) - x_m(t)) + K_{d_m}(\dot{x}_e(t) - \dot{x}_m(t)) - K_{f_m}(\hat{F}_e(t - T_2) + \hat{F}_h(t))$$

$$\ddot{x}_s(t) = K_{p_s}(x_m(t - T_1) - x_s(t)) + K_{d_m}(\dot{x}_m(t - T_1) - \dot{x}_s(t)) - K_{f_m}(\hat{F}_h(t - T_1) + \hat{F}_e(t))$$

where $x_e, x_m,\ \dot{x}_m,\ \ddot{x}_m$ are the estimated position of the slave and position, velocity and acceleration of the master manipulator respectively. $\hat{F}_e,\ \hat{F}_h$ denote the estimated environment and human forces and the subscript s stands for the slave manipulator. The authors choose the PD control gains relatively large at $K_p = 900,\ K_d = 60$, but keep the force control gain only at $K_f = 1$. During the simulations these gains were tuned to be $K_p = 90,\ K_d = 20,\ K_f = 2$ and the cut-off frequency of CDOB and DOB were chosen to be $g = 1250\ rad/sec$ to produce the following results.

The first simulation demonstrates a free motion scenario where the slave robot tracks the master robot freely. Figure 4.4 shows the results of the simulation. The tracking outperforms the P-like controller. The measured

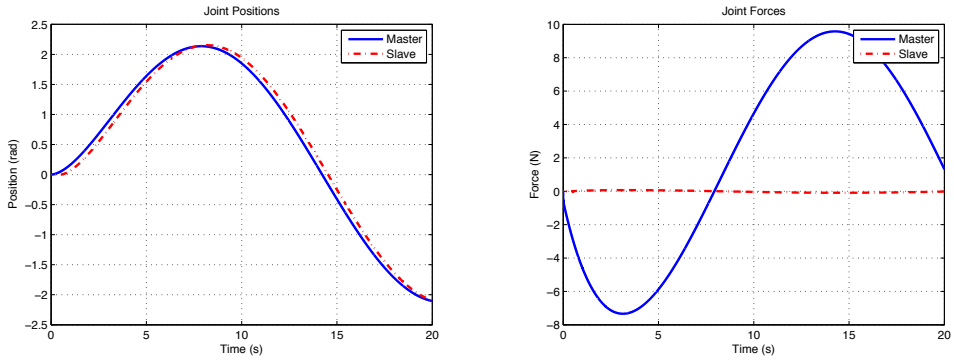

Figure 4.4: 1-DOF CDOB free motion simulation

tracking error is approximately 0.02 *rad*. A small oscillation around $F = 0$ can be observed in the estimated environment force, albeit the free motion scenario. This is due to the difference between external disturbance estimated by DOB and the computed forces based on nominal parameters for the RTOB estimation. The parametric uncertainties introduced to the simulation cause this difference. Wall model is unchanged from the previous contact simulation. The results for the contact simulation are given in Figure 4.5. Tracking is successful until contact with the obstacle ($t \simeq 5$ *sec*), at which point the slave stops its movement and the master overshoots the position of the obstacle by 0.25 *rad*. After approximately 0.5 *sec*, similar to the amount of delay in the communication channel, the master position is retracted by the environment force demonstrating the force reflection in the system. The delay is expected since the master can only feel the delayed force signal from the communication channel. The reflection of forces in the

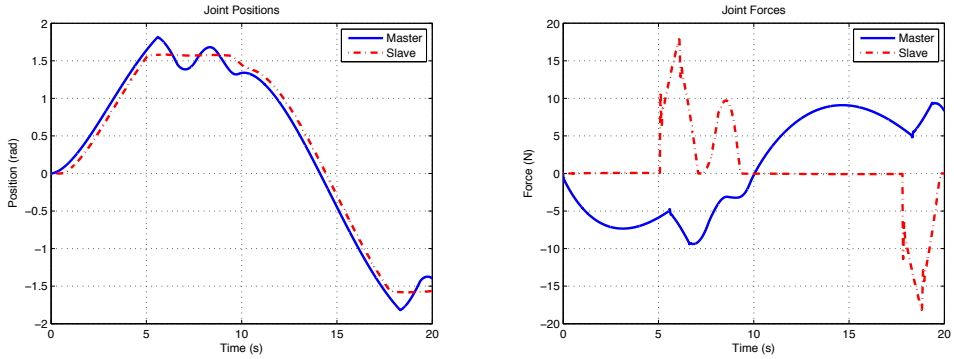

Figure 4.5: 1-DOF CDOB contact simulation

system is also visible in the force estimations. Between $t \simeq 5.5$ *sec* and $t \simeq 9.5$ *sec* the operator force increases to compensate for the environment force, but is overcome by the environment force peaking to approximately 18 N. The same phenomenon is observed after $t \simeq 17$ *sec* when the slave contacts the second obstacle. After oscillating around the position of the obstacle, the master leaves the obstructed zone at $t \simeq 19$ *sec* and the slave continues tracking until it contacts the second obstacle. The results show that the system is stable and environment forces are reflected to the operator.

4.1.3 PROB Simulations

Finally, the same scenarios are simulated using the proposed control architecture and delay compensation method. The control gains and cut-off frequency of the DOBs used in the CDOB simulations are unchanged at $K_p = 90,\ K_d = 20,\ K_f = 2,\ g = 1250\ rad/sec$. The results of the free motion simulation are given in Figure 4.6. The slave position tracks the master position with an error of less than 0.02 rad, with better performance than the

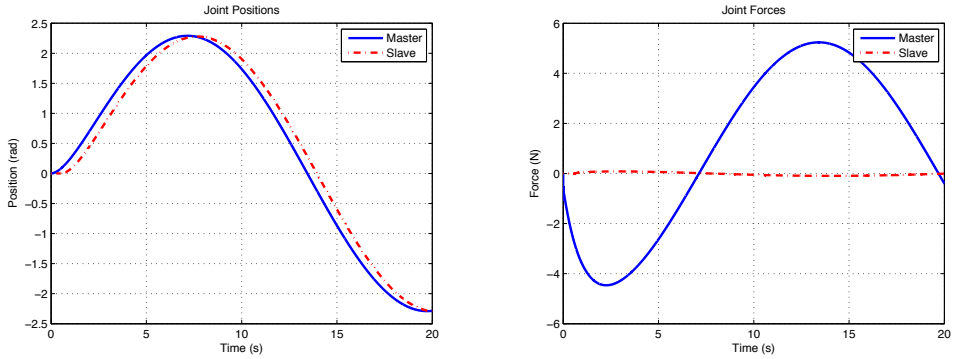

Figure 4.6: 1-DOF PROB free motion simulation

CDOB simulations. Force estimation oscillations are also visible in the results. The contact simulation is also repeated using the proposed method and the results are presented in Figure 4.7. Both the master and slave responses

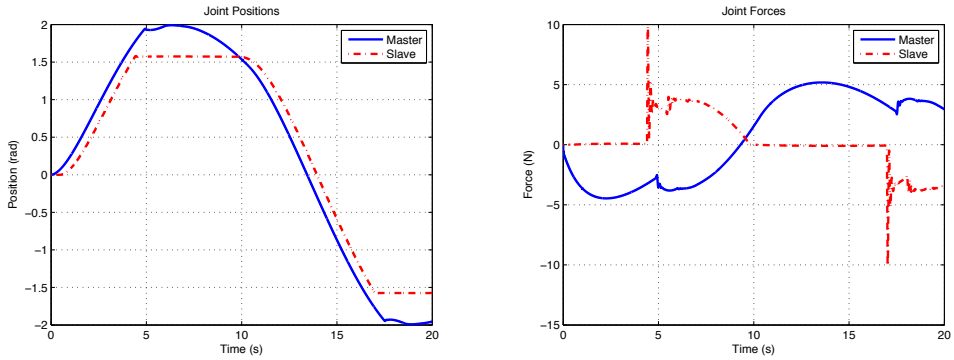

Figure 4.7: 1-DOF PROB contact simulation

vary from the CDOB simulation. The overshoot of the master position is greater, at approximately 0.42 *rad*, and it does not oscillate around the obstacle position. The master trajectory is smoother. It is also observed that the slave response is faster than the CDOB simulation. The contact with the wall occurs at $t \simeq 4.5$ *sec* instead of $t \simeq 5$ *sec*, a difference approximately equal to the amount of delay in the communication channel. This

observation supports the conclusion in Section 3.5 that the predictor observer estimates the future of the slave system ($\lim_{t\to\infty}\omega_e(t) = \lim_{t\to\infty}\omega(t+T_1(t))$) thus eliminates delay. The control signals are computed for an undelayed state of the slave and a faster response is obtained from the slave.

4.2 2-DOF Pantograph Robot Simulations

The performance of the proposed method is further tested with simulations of a nonlinear 2-DOF pantograph robot. The pantograph robot is modeled as consisting of four identical lightweight uniform rod links. The moment of inertia of the rods are calculated for with the assumption that axis of rotation is at the end. Moment of inertia and friction at the joints are not considered for simplicity. The parameters of the pantograph robot model are given in Table 4.2. The parameters of the motors (active joints)

Table 4.2: 2-DOF Pantograph Robot Parameters

	Mass (g)	Length (mm)	Inertia (gcm^2)
Link 1	30	200	4000
Link 2	30	200	4000
Link 3	30	200	4000
Link 4	30	200	4000
Link 5	-	120	-

are unchanged from the 1-DOF simulations, and a parametric uncertainty of 10% is added to the motor parameters. For simplicity and comparability of the results, a sinusoidal reference with an amplitude of $\pi/2$ rad and frequency of $1/15$ rad/sec is given to both joints in the joint space. This reference translates as an arc in the work space. In the results presented in

this section, a single cycle representative of the work space trajectory is given for clarity.

4.2.1 P-like Controller Simulations

Although it is not suggested in the authors' work, the nonlinear pantograph models are linearized using disturbance observers in an effort to make the results comparable to the other two methods which use disturbance observers. Due to the increased nonlinearity of the system, control gains are tuned to be $K_m = K_s = 15$, $B_m = B_s = 6.5$, satisfying the inequality. The results of a free motion simulation are given in Figures 4.8-4.10. The track-

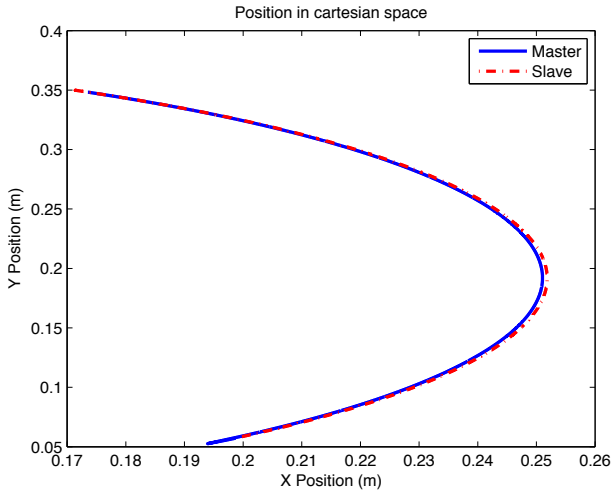

Figure 4.8: Pantograph P-like controller free motion simulation

ing performance is successful, with the slave position exceeding the master position slightly in the x-axis at the peak of the trajectory. For the contact simulation, a stiff wall is modeled at $x = 0.2\ m$ as a spring with a spring constant of $K = 2000\ N/m$. The results are presented in Figures 4.11-4.13. The slave motion in the x-axis stops during contact with the wall while

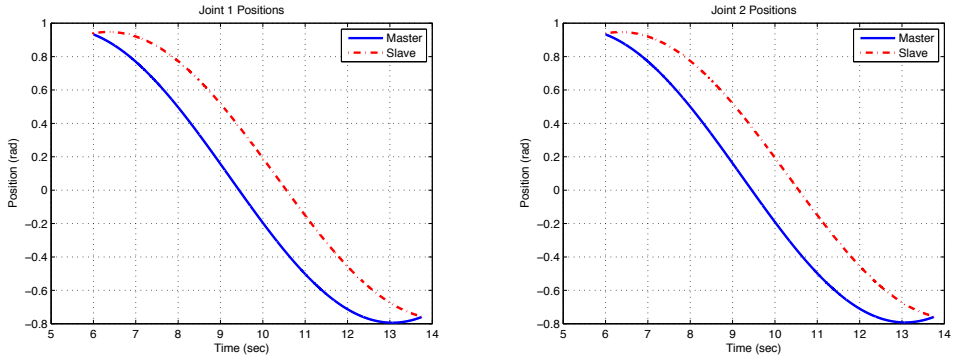

Figure 4.9: Joint positions for Pantograph P-like controller free motion simulation

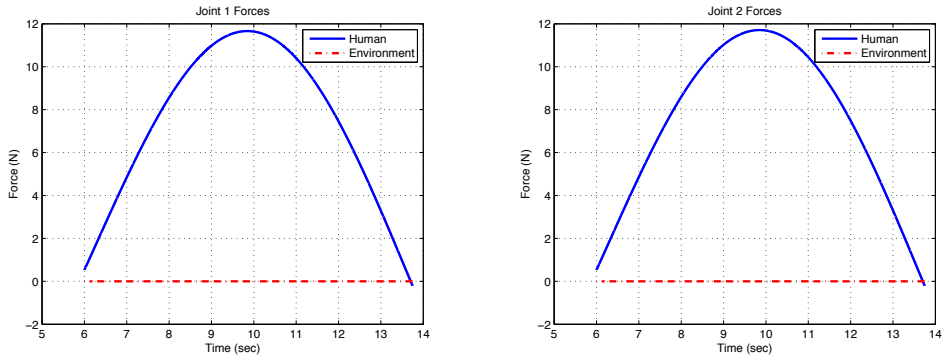

Figure 4.10: External forces on the joints for Pantograph P-like controller free motion simulation

it continues in the y-axis. This is expected since the obstacle is modeled as a frictionless wall on the x-axis. Master x position exceeds the obstacle position and repeats its trajectory in the free motion simulation, as a result of the non-transparent nature of the controller. In Figure 4.13, it is observed that the environment forces applied to the two joints are asymmetric. This is due to the fact that environment force is calculated in cartesian coordinates and mapped to the joint space using the Jacobian matrix of the pantograph model.

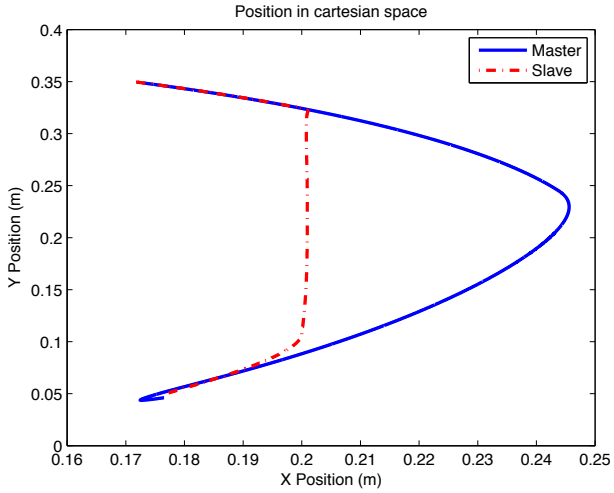

Figure 4.11: Pantograph P-like controller contact simulation

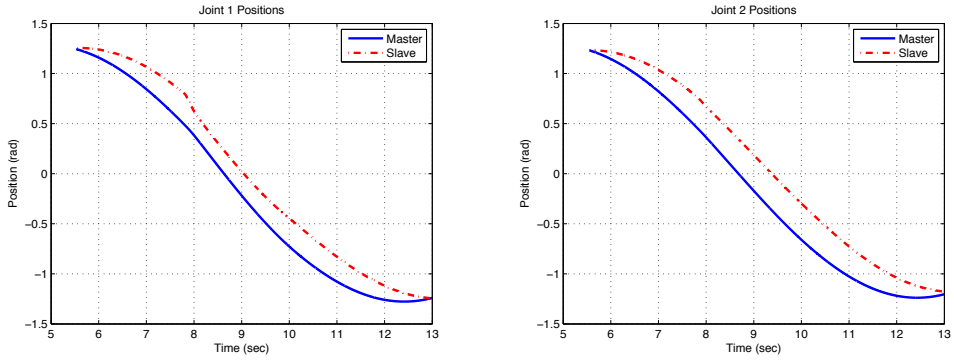

Figure 4.12: Joint positions for Pantograph P-like controller contact simulation

4.2.2 CDOB Simulations

The communication disturbance observer method is applied to the pantograph model, albeit the authors merely use a pair of 1-DOF robot arms in their experiments. However, the method is expected to perform successfully since the nonlinear dynamics of the pantograph are linearized and in practice the controller controls two independent linear joints. Control gains are

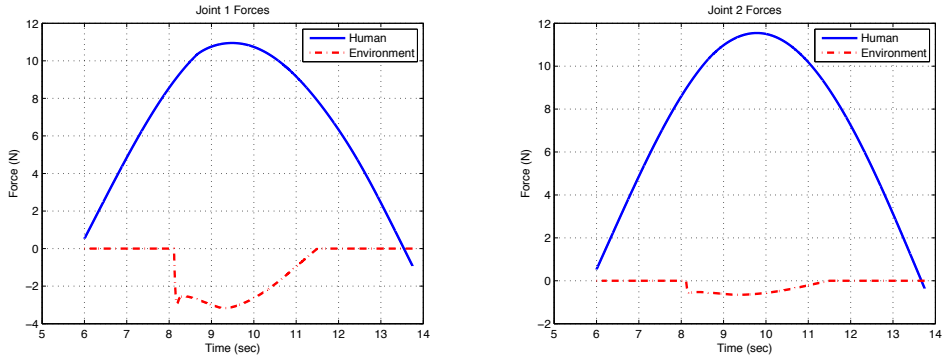

Figure 4.13: External forces on the joints for Pantograph P-like controller contact simulation

unchanged at $K_p = 90,\ K_d = 20,\ K_f = 2$, however the cutoff frequency of the disturbance observers are increased to $g = 1500\ rad/sec$ to account for the nonlinearities of the pantograph model. The results of the free motion simulation are shown in Figures 4.14-4.16. As in the 1-DOF simulations, the

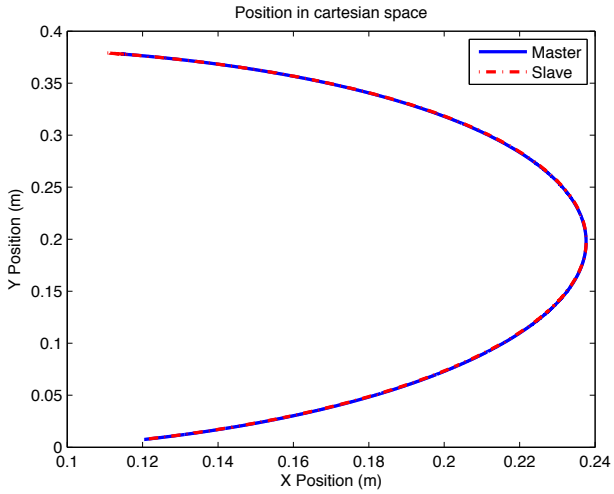

Figure 4.14: Pantograph CDOB free motion simulation

slave tracks the master trajectory exactly. The environment force oscillation can be observed in Figure 4.16. Contact simulation is repeated for the CDOB

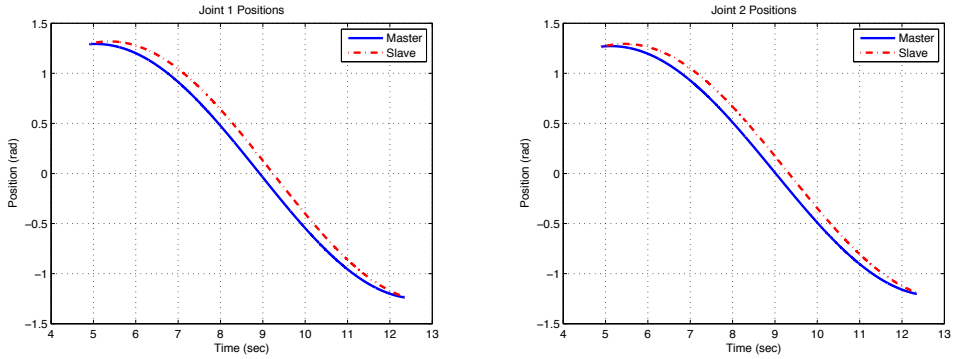

Figure 4.15: Joint positions for Pantograph CDOB free motion simulation

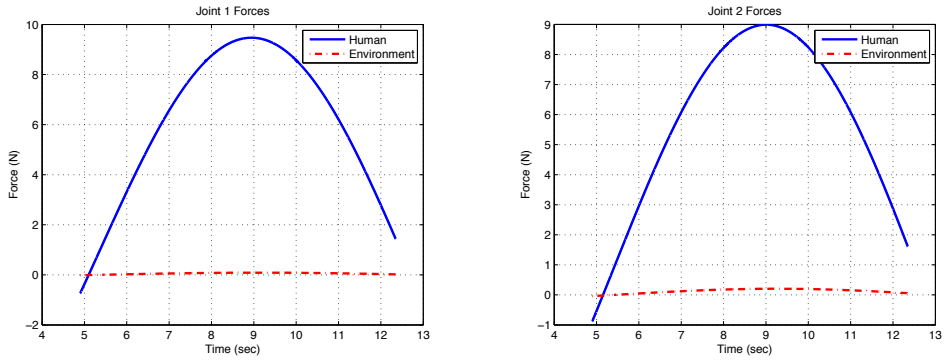

Figure 4.16: External forces on the joints for Pantograph CDOB free motion simulation

method and results are presented in Figures 4.17-4.19. The master and slave robot trajectories resemble the 1-DOF simulation. During contact with the obstacle, slave motion in the x direction stops while the master overshoots the obstacle position by approximately 3 cm at which point it is retracted by the delayed environment force feedback, demonstrating that transparency is achieved to a certain extent by reflection of environment forces in the system. After the force input, the master position undershoots the obstacle position, deflecting from its trajectory in the free motion simulation. The sluggish

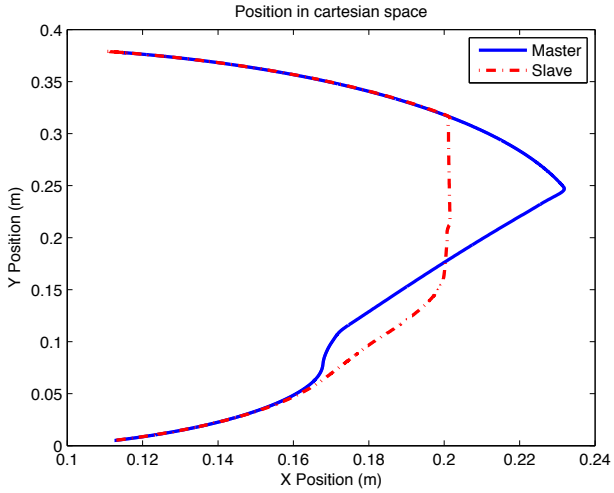

Figure 4.17: Pantograph CDOB contact simulation

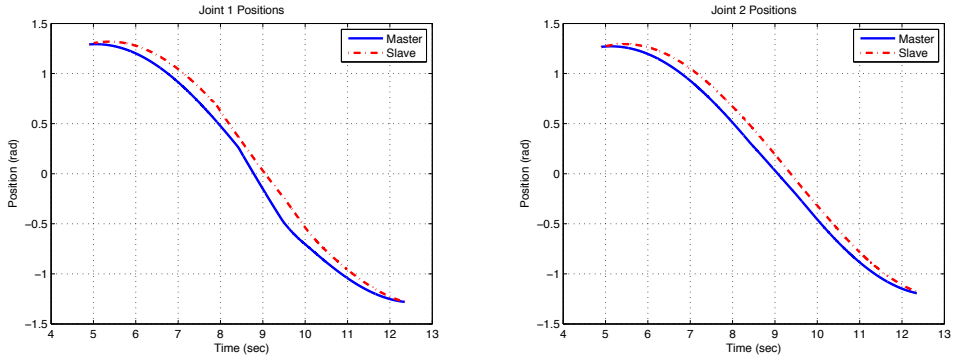

Figure 4.18: Joint positions for Pantograph CDOB contact simulation

response of the slave under this control architecture can be observed in this simulation. The slave does not immediately resume tracking the master once the master returns to the unobstructed zone. Master and slave trajectories eventually converge and slave resumes tracking the master successfully.

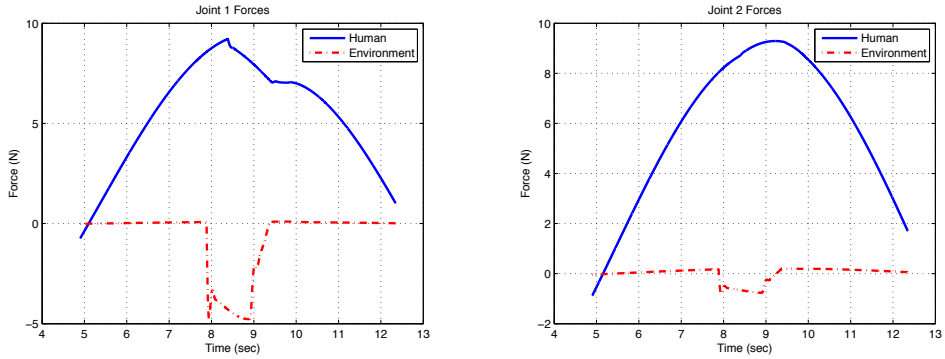

Figure 4.19: External forces on the joints for Pantograph CDOB contact simulation

4.2.3 PROB Simulations

Pantograph simulations are repeated for the proposed control architecture and delay compensation method utilizing predictor observer. These simulations also serve as a basis for the experiments presented in this work. The control gains are chosen as the same in CDOB simulations, at $K_p = 90,\ K_d = 20,\ K_f = 2,\ g = 1250\ rad/sec$. Results of the free motion simulation are given in Figures 4.20-4.22. Tracking is successful except for the extrema in the x direction. At the extrema, slave trajectory overshoots the master trajectory by approximately 0.5 cm. This error is due to the parametric uncertainties introduced to the simulations. Since the slave control input is computed at the master side based on the predictions of the PROB on a nominal slave model, parametric uncertainties yield a difference between real and estimated positions of the slave. Oscillation of the force estimation around $F = 0$ is visible. Finally, the contact scenario is simulated using the proposed architecture and the results are presented in Figures 4.23-4.25.

The master trajectory overshoots the obstacle position by approximately

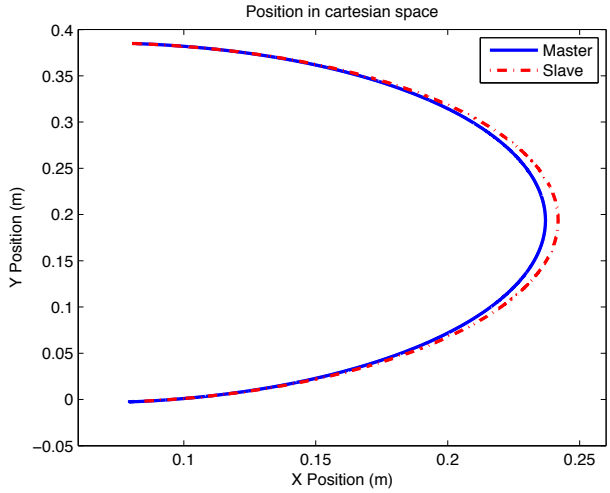

Figure 4.20: Pantograph PROB free motion simulation

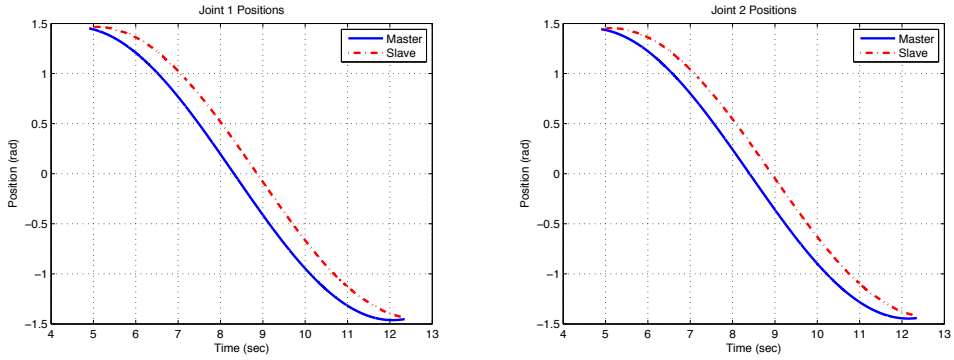

Figure 4.21: Joint positions for Pantograph PROB free motion simulation

3 *cm*, in accordance with the 1-DOF results and the results of the CDOB method. Once the delayed environment force reaches the master side, both the trajectory and operator force are affected, demonstrating a degree of transparency of the system. Master position is retracted towards the obstacle and it resumes its original trajectory from free motion simulation. The trajectory does not deflect as in the CDOB contact simulation, another advantage of the proposed method over CDOB. Also, as in the 1-DOF contact

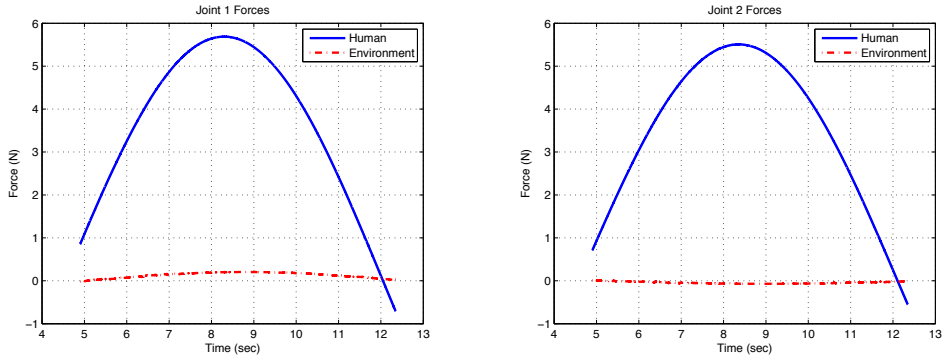

Figure 4.22: External forces on the joints for Pantograph PROB free motion simulation

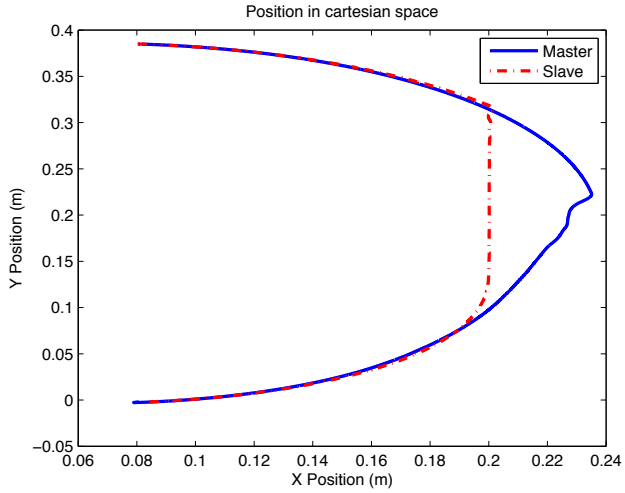

Figure 4.23: Pantograph PROB contact simulation

simulation, retraction of the master position is smoother than the CDOB method. This is due to the proposed control architecture that relies on the estimations from the PROB. The predictor observer depends on delayed environment force information and inevitably makes the faulty prediction that the slave is moving until the force information is received through the communication channel. It is at this point that the estimated slave trajectory

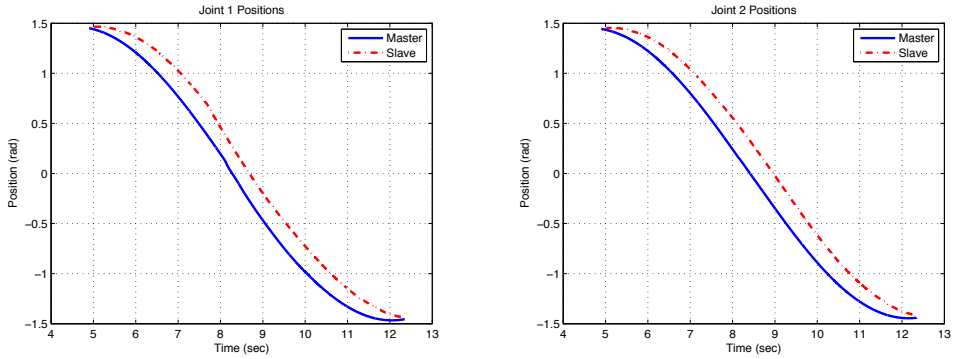

Figure 4.24: Joint positions for Pantograph PROB contact simulation

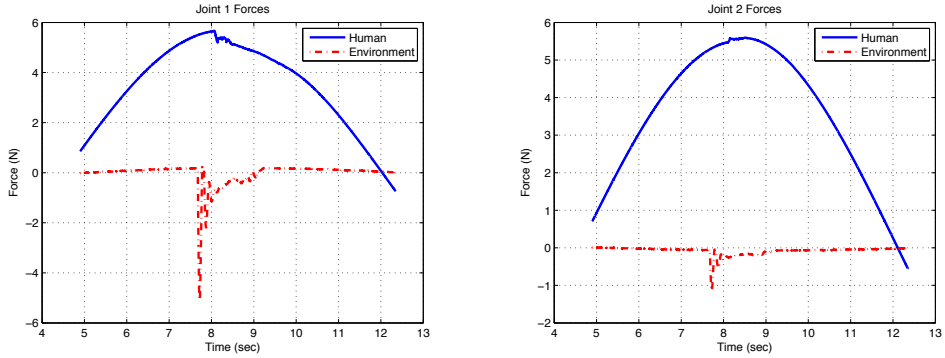

Figure 4.25: External forces on the joints for Pantograph PROB contact simulation

comes to a halt and starts retracting the master position towards itself. For the purposes of the two controllers at the master side, the obstacle exists at a position slightly greater than its actual position. As a result of the discrepancy, the controller does not exert a large force on the master to retract it and does not cause an undershoot as in the CDOB case. The trajectory of the master is smoother and it does not deflect to an undesired position as observed in the CDOB simulation. This conclusion is also supported by the fact that the master position is retracted approximately 1 *cm* and then

continues its trajectory.

4.3 Discussion

The simulation results presented in this chapter reveal that the proposed method delivers stable and force reflecting teleoperation. The P-like controller method delivers stable teleoperation, as claimed by the authors, however it is not transparent. The results of the proposed method outperforms the P-like controller in both 1-DOF and 2-DOF contact simulations. Force reflection is clearly visible in the force estimations and the master position retracts to the obstacle position, demonstrating a desirable behavior. Compared to the CDOB approach, the master trajectories are smoother during the slave's contact with environment and the master is not forced into a different trajectory than the free motion scenario. The claim in Section 3.5 that the predictor observer estimates the future states of the slave is demonstrated in the simulations as well, by the responsiveness of the slave system.

The stable and smooth response of the master system to the environment forces show that the proposed method achieves a tradeoff between stability and transparency that provides more stable contact behavior for the master. A degree of transparency is preserved while the master is smoothly retracted towards the obstacle, as opposed to the oscillatory retraction behavior demonstrated in CDOB simulations.

Chapter V

5 Experimental Results and Discussions

After obtaining satisfactory tracking performance in the simulations, experiments are carried out to test the performance and robustness of the proposed control architecture in physical bilateral teleoperation. Two experimental test beds are used for the experiments: a pair of 1-DOF revolute arm manipulators and a pair of 5-link, 2-DOF pantograph robots (Fig. 5.1). The testbeds are designed and assembled at the Sabancı Mechatronics laboratory to be used in a bilateral teleoperation system as master and slave systems. For a more detailed analysis of the dynamics of the pantograph

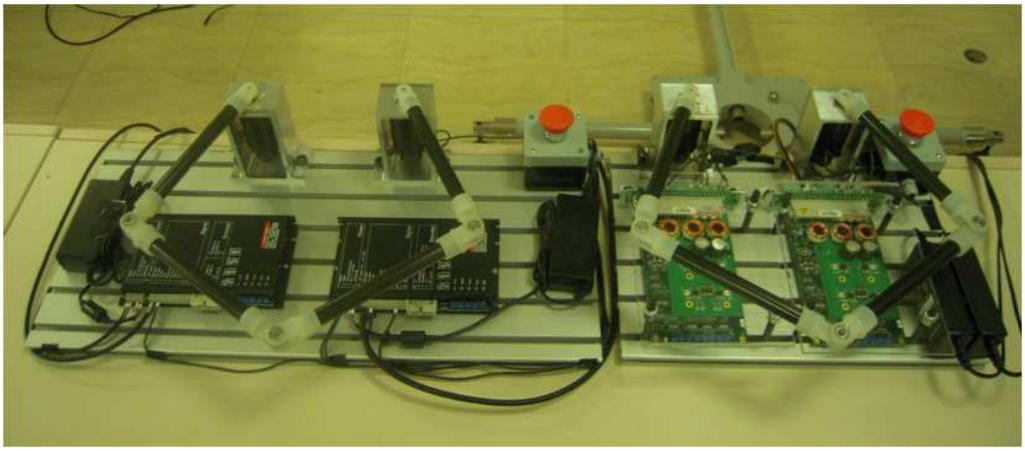

Figure 5.1: Master and slave pantograph robots

robot, please refer to [54]. The nonlinear dynamical equations of pantograph

robots are linearized using DOBs. Three channel control architecture utilizing the predictor observer is implemented to control the pantograph robots and the performance of the proposed approach in tracking stability and force reflection under time delay are investigated. The pantograph robots are controlled by a dSpace 1103 real-time control card. The experimental setups are demonstrated in Figure 5.2. In the experiments, the end-effector positions

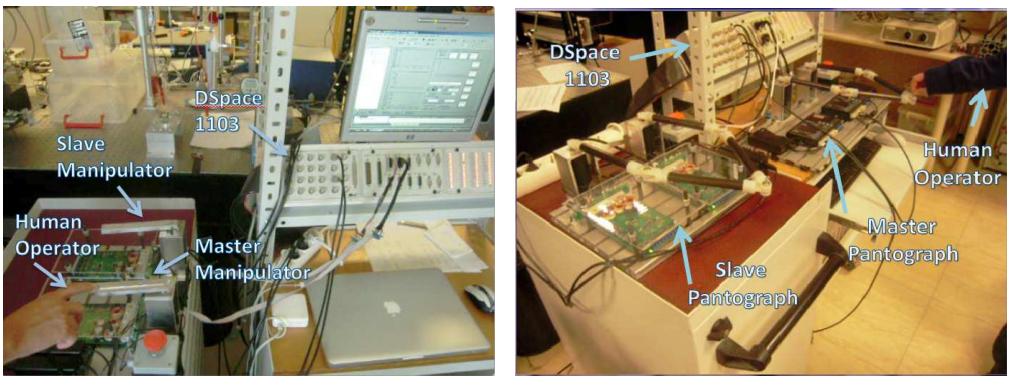

Figure 5.2: 1-DOF and pantograph robot experimental setups

of the pantographs in $x - y$ plane, joint angles and estimated forces at the joints are examined. The aim is to achieve stable tracking of the master trajectories while reflecting environment forces to the human operator.

5.1 Artificial Delay Experiments

The communication channel is modeled in Matlab/Simulink by introducing a variable time delay characterized by a normally distributed random variable with a mean of 0.5 *sec* and standard deviation of 0.025 *sec* using Matlab's Time-Variable Delay block. The Matlab/Simulink model is run in real-time on the dSpace 1103 control card. The control parameters of the modified 3-channel controller (K_p, K_d, K_f) are selected to be the same as in

simulations $K_p = 90$, $K_d = 20$ and $K_f = 2$ for both joints. The cut-off frequency of the low-pass filter, $G(s)$, used in the DOB and RTOB estimations is set to $g = 1250\ rad/sec$.

The delay compensation method is first tested on the 1-DOF experimental setup. Human operator moves the master arm in an arbitrary trajectory and the tracking of the slave is observed. In this experiment the slave does not contact the environment. Figure 5.3 shows the master and slave joint angles, and estimated forces at the joints. Slave tracks the master successfully with

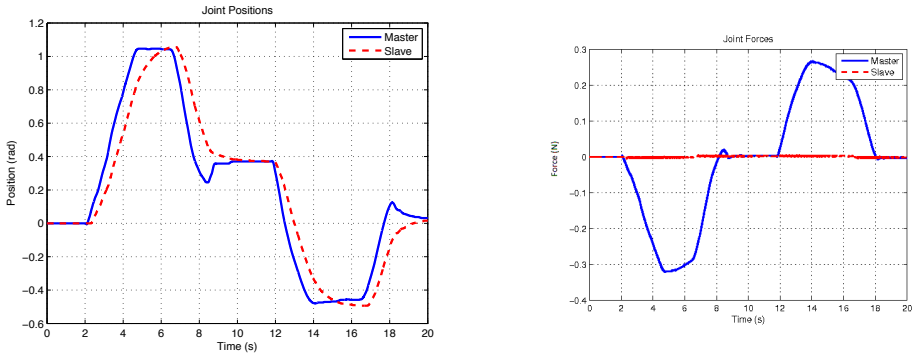

Figure 5.3: 1-DOF free motion experiment

an approximate delay of 0.5 *sec*. It is observed that the slave trajectory is smoother at the corners than the master trajectory (at $t \simeq 8.5\ sec$ and $t \simeq 18\ sec$), however the error does not exceed 0.1 *rad*. As expected, the force estimations at the slave joint oscillate around $F = 0$ as in the simulations due to the internal disturbances at the joint and the parametric uncertainty. As explained in the RTOB section, net external force estimation is as precise as the estimation of other terms in the total disturbance.

Next, the 1-DOF system is tested under contact with the environment and same delay conditions. Figure 5.4 shows the system setup and the vertical

rod used as an obstacle. Slave contacts the obstacle at $t \simeq 18$ *sec* and stays in contact until $t \simeq 26$ *sec*. The results are shown in Figure 5.5 The tracking

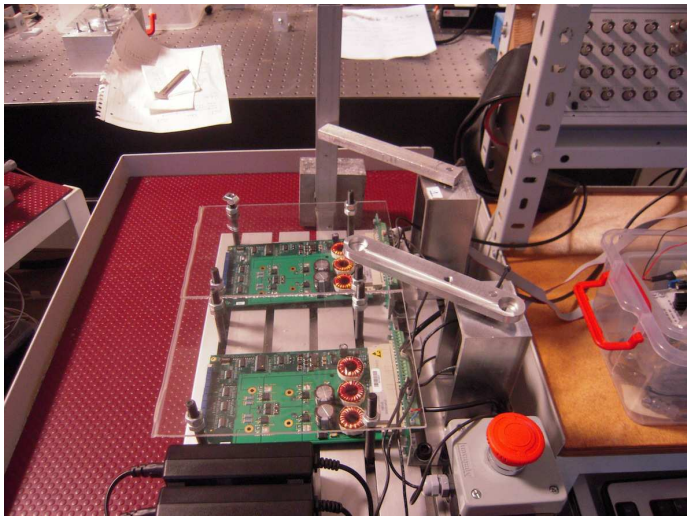

Figure 5.4: 1-DOF contact experiment setup

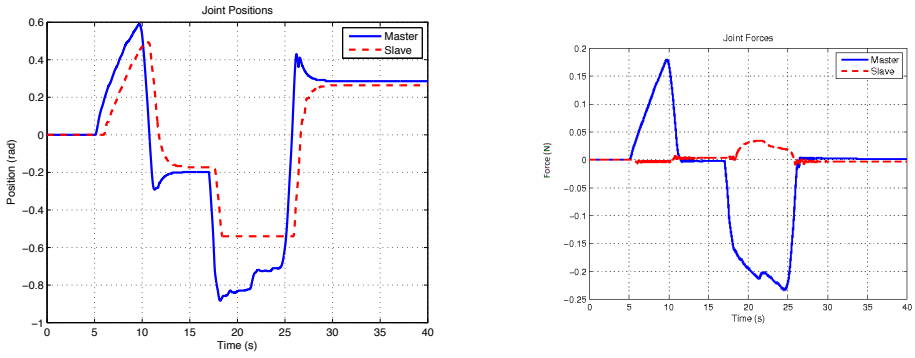

Figure 5.5: 1-DOF contact experiment

performance in the unobstructed zone is similar to the previous experiment. The tracking errors at the corners do not exceed 0.1 *rad*. The environment force is clearly visible between $t \simeq 18$ *sec* and $t \simeq 26$ *sec* and it is reflected to the operator. Although the magnitude of the operator force increases in this

timeframe, the master position is observed to be retracting to the obstacle position. This shows that the operator needs to exert a larger force to keep the master position beyond the obstacle position. This force is the reflection of the environment force to the operator.

After validating the performance of the control architecture in 1-DOF experiments, the nonlinear pantograph robots are introduced for further testing. The delay characteristics and control parameters are unchanged, but the cut-off frequency of the DOBs and RTOBs is increased to $g = 1500\ rad/sec$ to compensate for the increased complexity of the system. In the first experiment, a closed curve is drawn by the operator. There is not any contact with environment. The end-effector positions, joint positions and estimated forces at the joints are shown in Figures 5.6-5.8. As shown in Figure 5.6,

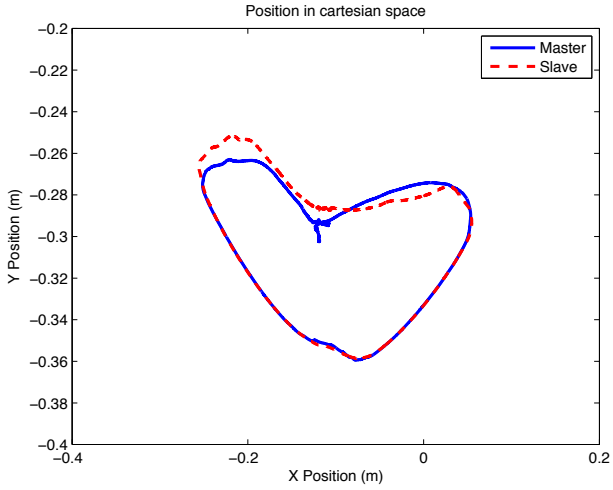

Figure 5.6: Pantograph free motion experiment: Tracking a closed curve

the end-effector of slave pantograph (dashed line) tracks the end-effector of master pantograph (solid line) with a maximum error of approximately 2 cm. It should be noted that the oscillations about $F = 0$ in the force estimation

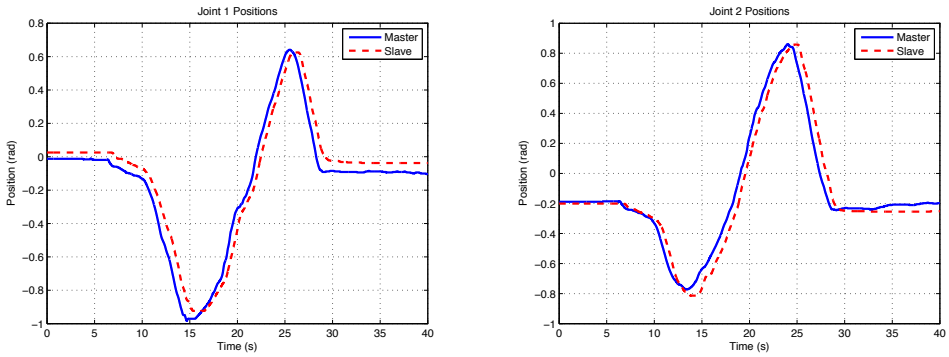

Figure 5.7: Joint positions for Pantograph free motion experiment

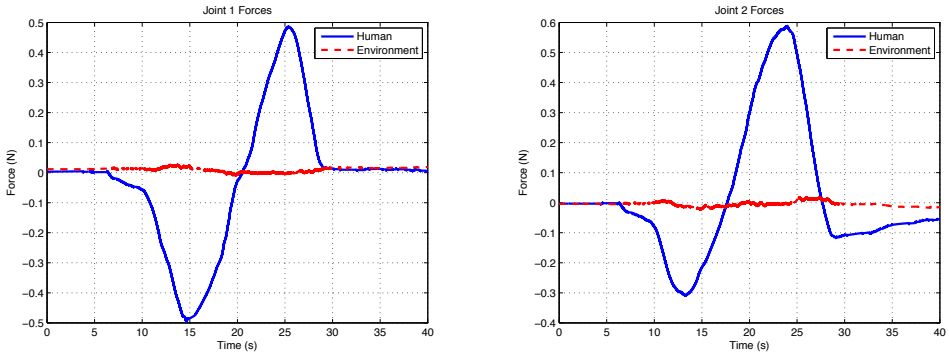

Figure 5.8: External forces on the joints for Pantograph free motion experiment

at the joints of the slave pantograph are greater than that of the 1-DOF case. This is due to the increased number of nonlinear terms and coupling forces at the passive joints of the pantograph that are more difficult to be modeled accurately for the RTOB output. The decreased accuracy causes a greater magnitude of total disturbance to be estimated as net external force. However, as will be seen in contact experiments, the magnitudes of the forces during contact are significantly greater than the oscillations and realistic estimations can be obtained.

In another experiment, a spiral reference (an open curve) is drawn by the operator. The reason for choosing a spiral shape for reference to the slave is the observation that tracking errors increase during circular motions, therefore a spiral trajectory is considered as a worst case scenario for tracking performance. Results of the experiment are given in Figures 5.9-5.11.

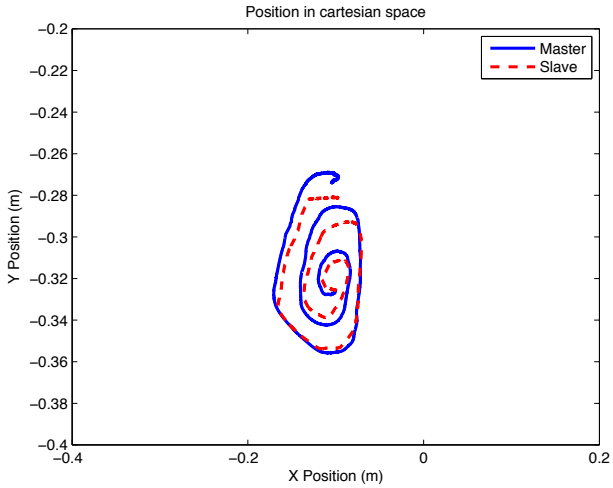

Figure 5.9: Pantograph free motion experiment: Tracking a spiral trajectory

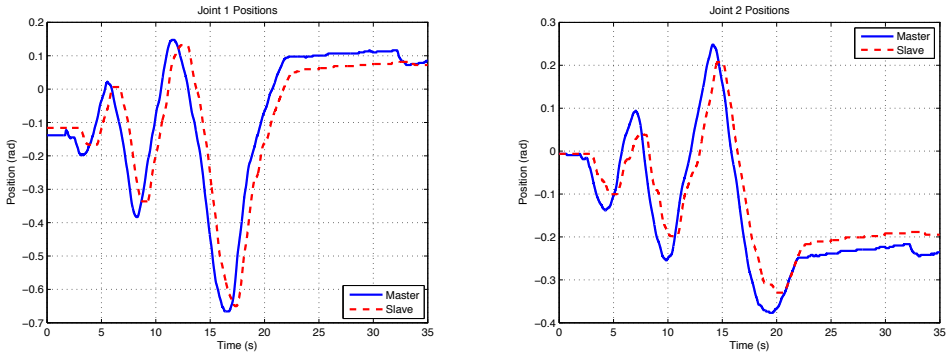

Figure 5.10: Joint positions for Pantograph free motion experiment

The reason for the relatively large margin of error is evident from the joint

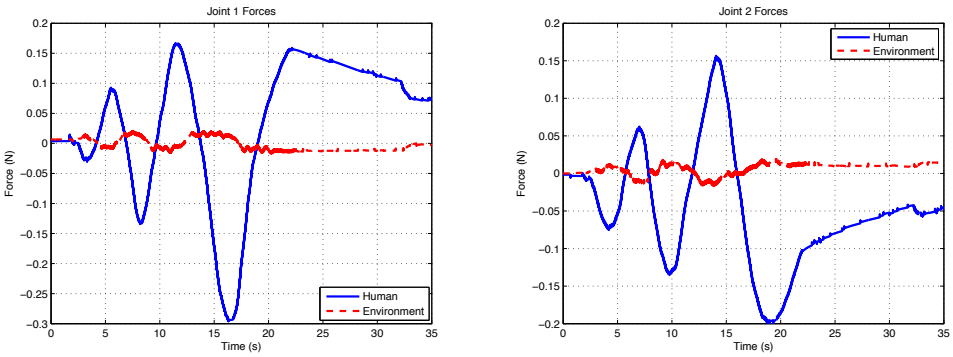

Figure 5.11: External forces on the joints for Pantograph free motion experiment

positions in Figure 5.10. The circular motion of the end-effector requires frequent changes in the direction in the motion of the joints. As observed in the 1-DOF experiments, tracking error increases at the corners of the joint position. However, as observed in Figure 5.9, the tracking error stays less than 2 *cm* during the experiment.

After the free motion experiments, contact experiments are conducted to observe the performance of the control architecture with nonlinear systems under contact with environment. In this experiment, a wall obstacle is introduced to the experimental setup. The obstacle consists of a wrench fixed horizontally to a vertical column. Figure 5.12 shows this experimental setup. Results of the first contact motion experiment are given in Figures 5.13-5.15. Tracking in the unobstructed zone is successful, with errors much less than 2 *cm*. As seen in Figure 5.13, master position enters the obstructed zone while the slave position cannot. Similar to the simulation results, slave motion stops in the perpendicular direction to the wall while tracking continues in the parallel direction. Once the master position returns to the unobstructed zone, tracking continues successfully. Contact forces are

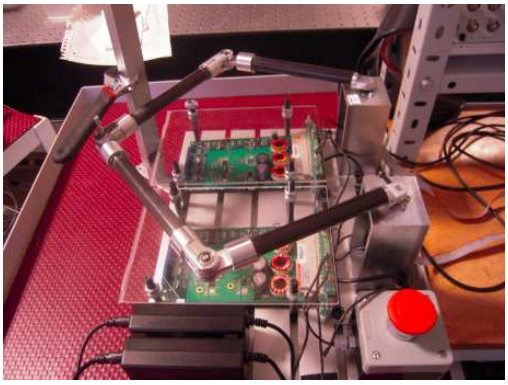

Figure 5.12: Pantograph contact experiment setup

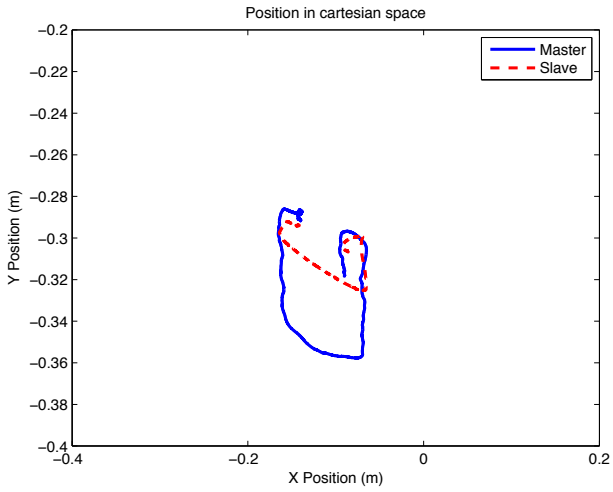

Figure 5.13: Pantograph contact experiment: Wall contact

clearly visible between $t \simeq 10$ *sec* and $t \simeq 25$ *sec* in Figure 5.15. Oscillations about $F = 0$ were observed to have magnitudes less than 0.03 N in the free motion experiments, but reach magnitudes of 0.2 N in during contact. We can conclude that the amount of disturbance that is added to the force estimations is insignificant with respect to the total force estimations. It can be

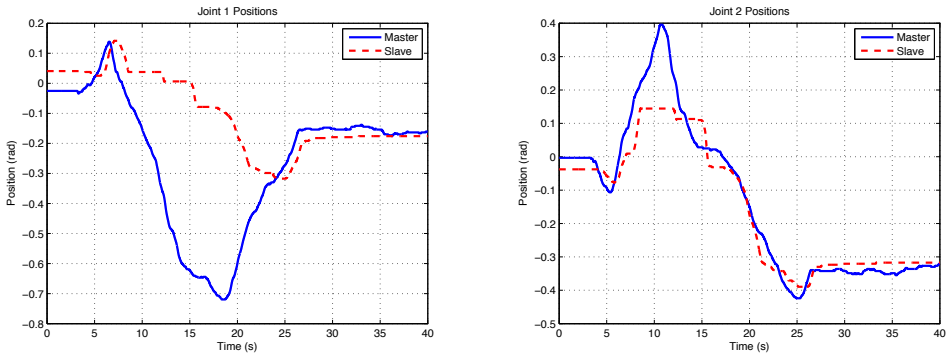

Figure 5.14: Joint positions

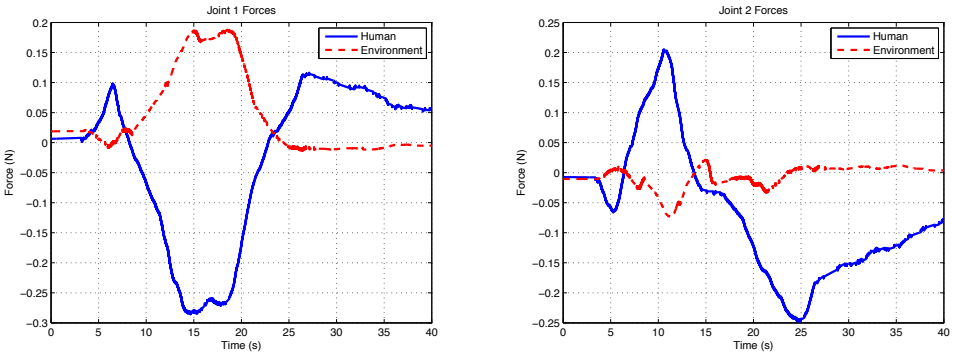

Figure 5.15: External forces on the joints

seen that the environment force estimated at the slave side is reflected to the master side, thus providing a degree of transparency in the system. Master force between $t \simeq 10$ *sec* and $t \simeq 25$ *sec* in Figure 5.15a shows an increase from free motion forces and the trough and crest of the force estimations are reciprocals of each other. The similarities of the wave forms imply that the operator feels the environment forces.

In another contact experiment, the same wall obstacle is positioned at a different location in the workspace and the experiment is repeated. The results of the experiment are shown in Figures 5.16-5.18. The tracking

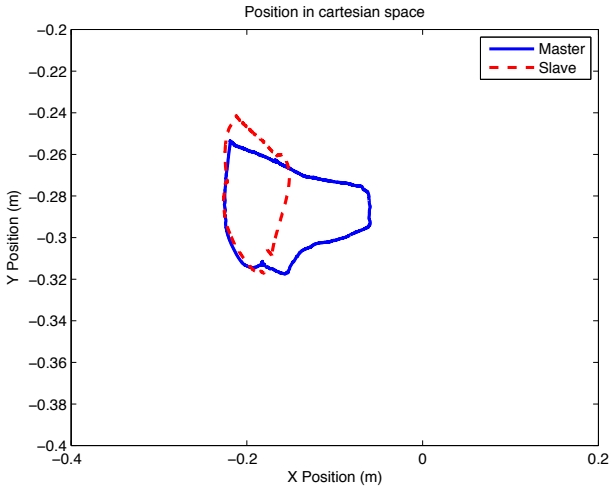

Figure 5.16: Pantograph contact experiment: Wall contact

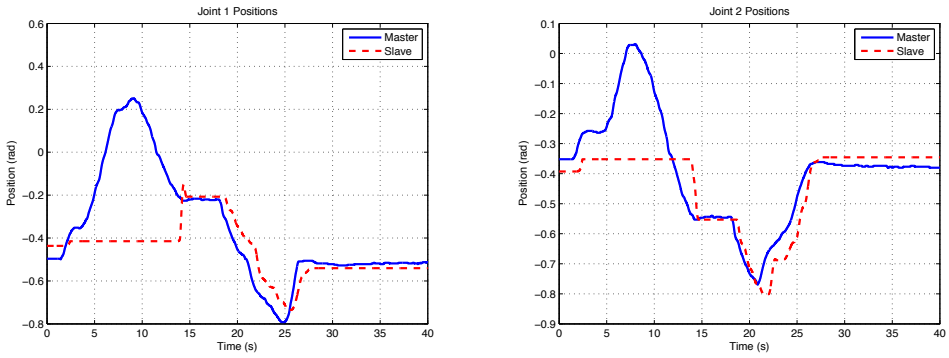

Figure 5.17: Joint positions

performance and contact behavior are very similar to the previous experiment. Albeit greater than the previous experiment, the tracking error in the unobstructed zone does not exceed 2 cm.

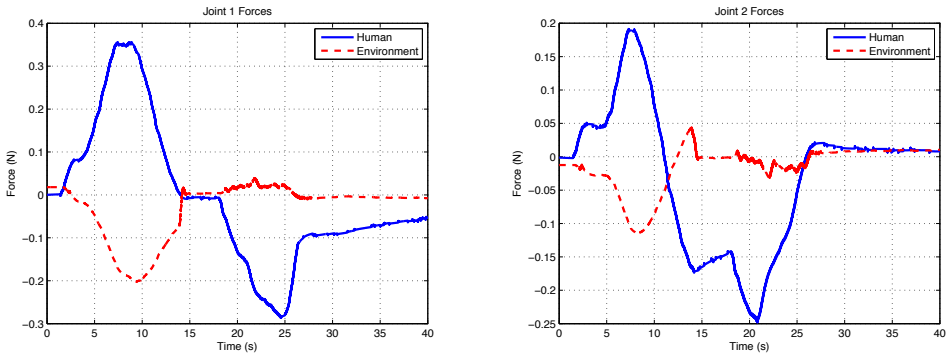

Figure 5.18: External forces on the joints

5.2 Internet Delay Experiments

After the performance of the proposed method under artificial delay is verified, the system is modified to replace Matlab's Time Variable Delay block with real delay from an internet connection. In order to achieve this, three computer programs are written in C++ language. The programs running at the master and slave sides read the slave control input, position and force signal values from the dSpace1103 card, send these signals to the opposite side and write the received signal values back to the dSpace1103 card, achieving the three channel control architecture. Since both master and slave system are connected to a computer at the Sabancı University campus, a third computer is necessary to merely bounce signals and introduce internet delay. All communication is executed using the User Datagram Protocol (UDP) due to its robustness and speed advantage over Transmission Control Protocol (TCP). The third computer is located in Beşiktaş, in the European side of Istanbul, providing a physical distance of approximately 100 km for the roundtrip delay.

During the experiments, it is observed that along with a time delay of ap-

proximately 150 ms, a sampling time problem is introduced to the exchanged signals. Although the dSpace1103 cards run at 1 kHz, received signals were measured to be at approximately 20 Hz. Figure 5.19 shows a 1 sec section of a position signal before and after transmission. The sampling problem

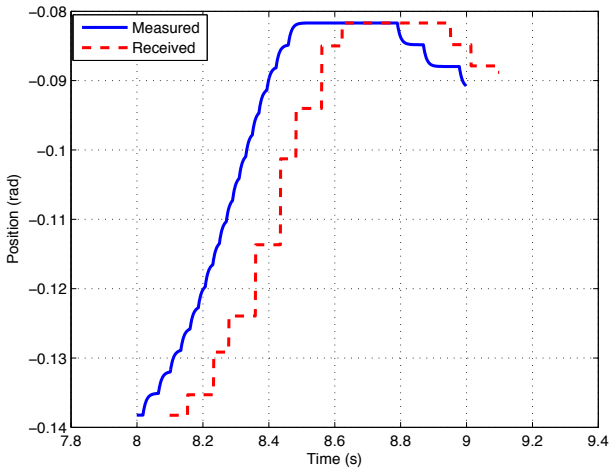

Figure 5.19: Position signal before and after transmission

extends the scope of test of the control architecture's robustness. As the results presented in the section show, performance degradation due to the sampling problem is insignificant. Experiments are performed with similar trajectories to the artificial delay experiments in order to make them comparable. Control parameters and cut-off frequency of disturbance observers remain unchanged at $K_p = 90$, $K_d = 20$, $K_f = 2$ and $g = 1250\ rad/sec$ for the 1-DOF manipulators and $g = 1500\ rad/sec$ for the pantographs. For the 1-DOF manipulators, only a contact experiment with the same setup shown in Figure 5.4 is presented. Results are shown in Figure 5.20 It is observed that the tracking error at the corners are about 0.2 rad, only slightly greater than artificial delay experiments. The main reason for this robustness

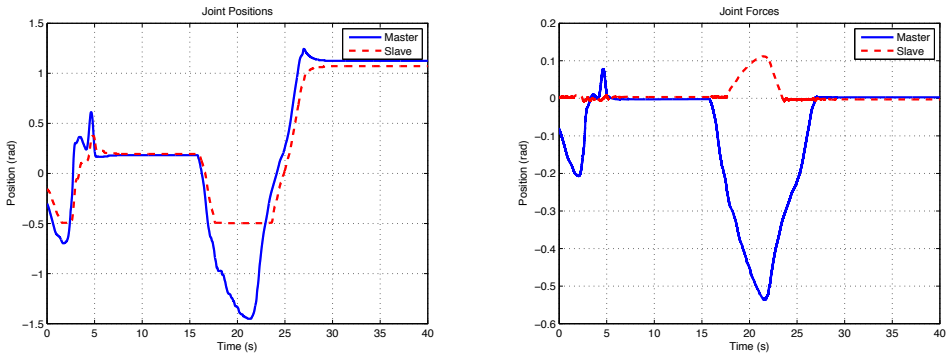

Figure 5.20: 1-DOF contact experiment

against sampling issue is the system architecture. Placement of both master and slave controllers and PROB at the master side enables all components of the system to run at the native sampling rate of 1 kHz. Although the PROB input is updated at 20 Hz, the slave controller is supplied with estimated slave position at a rate of 1 kHz. The down-sampling of the control input does not cause significant errors in the tracking.

After obtaining successful results for the 1-DOF manipulators, the pantograph experiments are repeated under internet delay. The results for closed curve tracking are given in Figures 5.21-5.23. As in artificial delay experiments, slave pantograph tracks the master position with an error less than 2 cm. The oscillatory behavior of the environment force estimation is also observed to be similar to the artificial delay experiments. The sampling problem does not induce a tangible performance degradation. The results for the open curve tracking experiment are given in Figures 5.24-5.26. It is observed that the tracking error increases at $t \simeq 22$ sec at which point the slave joint positions undershoot the master joint positions. The maximum tracking error is approximately 2 cm. However, this error is still bounded and only

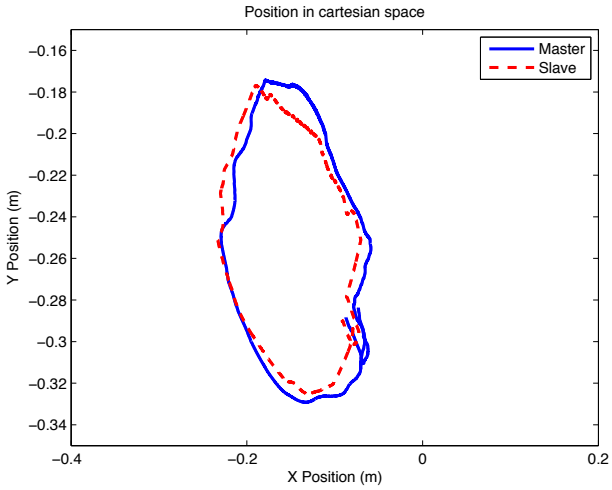

Figure 5.21: Pantograph free motion experiment: Tracking a closed curve

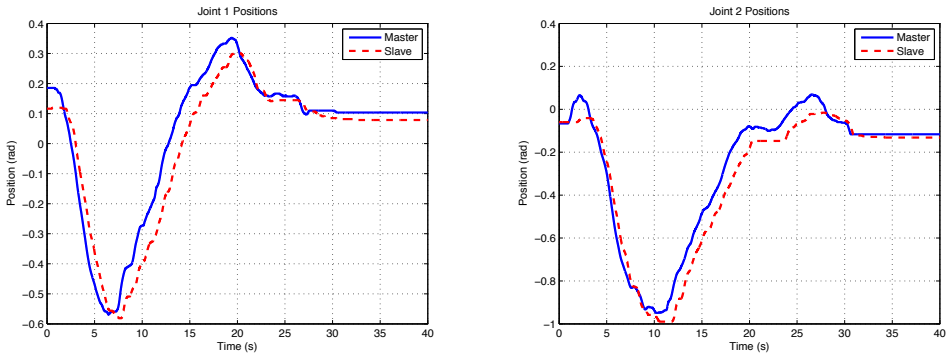

Figure 5.22: Joint positions

slightly greater than the errors encountered in artificial delay experiments. The contact experiments are also repeated using the same obstacle setup in Figure 5.12. The results are presented in Figures 5.27-5.29. Tracking in the unobstructed zone is achieved with a maximum error of about 1 cm. Force reflection can be observed in the reciprocal addition of the environmental force to the operator force in Figure 5.29b. After $t \simeq 16$ sec, estimated human force increases from 0.15 N to 0.3 N, equal to the peak of estimated

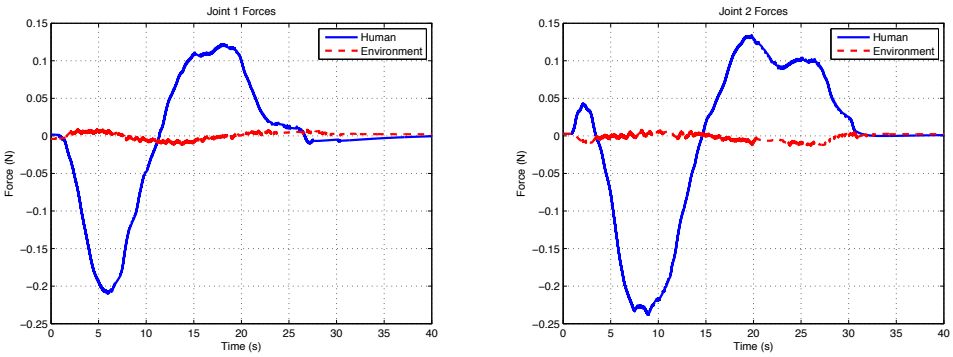

Figure 5.23: External forces on the joints

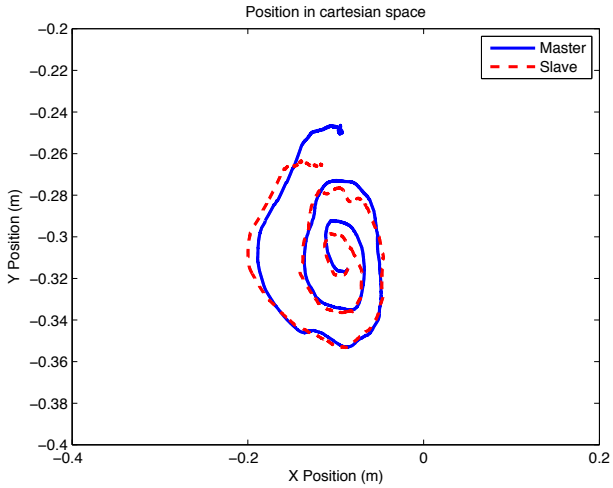

Figure 5.24: Pantograph free motion experiment: Tracking an open curve

environment force. The waveforms of the two signals are also reciprocals of each other.

Another contact experiment is carried out with a different contact setup. As shown in Figure 5.30 a vertical bar is placed in front of the slave pantograph and the end-effector contacts the obstacle at a single point. It does not move while in contact with the obstacle. The greek letter alpha is drawn by the operator and the slave pantograph contacts the obstacle at the inter-

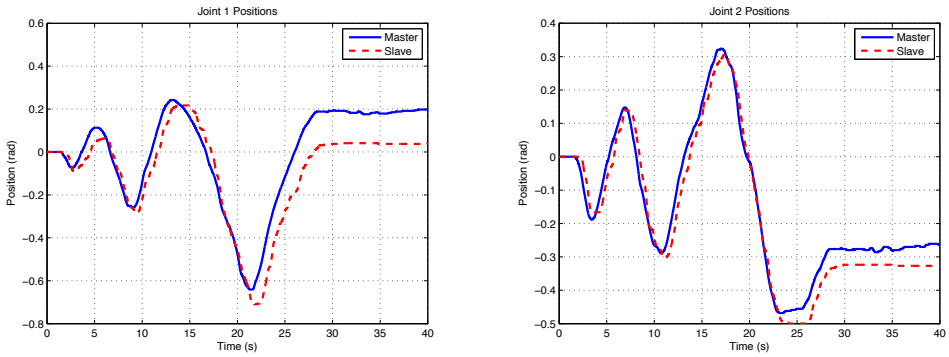

Figure 5.25: Joint positions

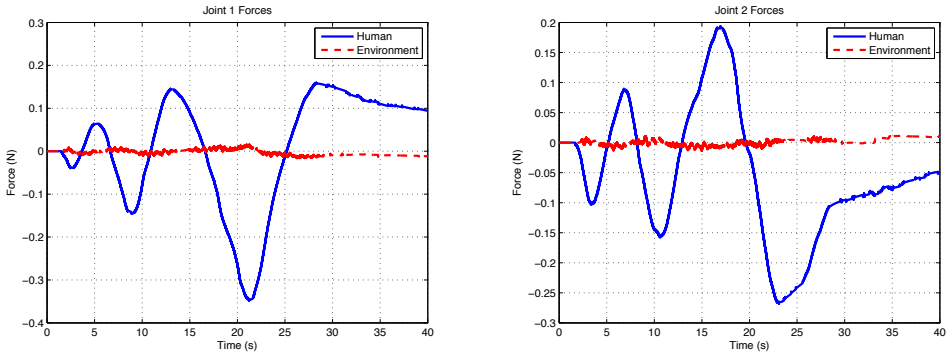

Figure 5.26: External forces on the joints

section point of the letter. The results are presented in Figures 5.31-5.33.

Tracking error in the unobstructed zone is larger than other experiments at approximately 2.5 cm. The contact forces are visible between $t \simeq 8$ sec and $t \simeq 13$ sec. It should be noted that the joint positions in Figure 5.32 are stationary during contact, since the motion of the slave completely stops during contact.

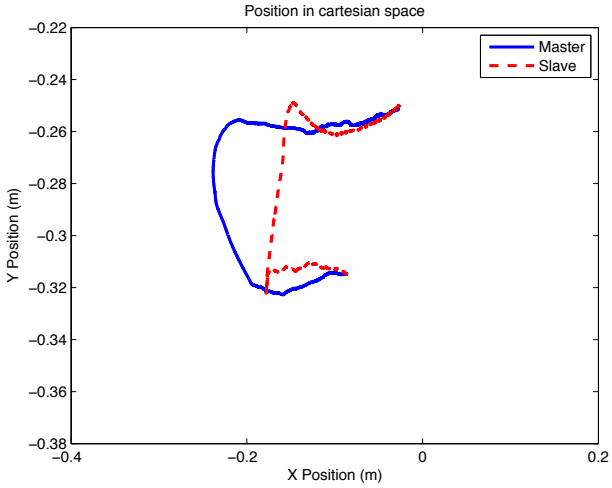

Figure 5.27: Pantograph contact experiment: Wall contact

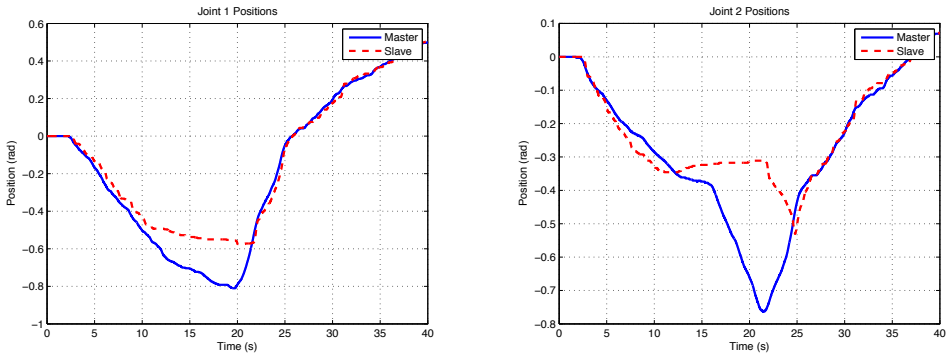

Figure 5.28: Joint positions

5.3 Discussion

Experimental results presented in this chapter indicate that the nonlinear dynamics of pantograph robots are successfully linearized and the parameter uncertainties in the system are adequately eliminated by the DOBs, which in turn allows the implementation of PROB for delay compensation and three channel control architecture for stable and force reflecting bilateral operation.

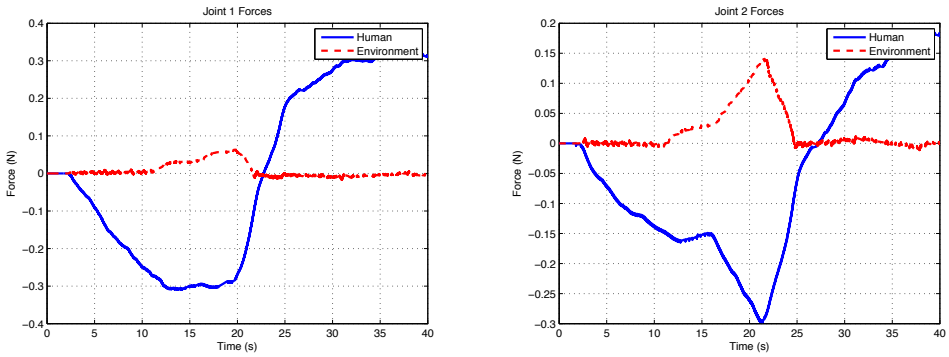

Figure 5.29: External forces on the joints

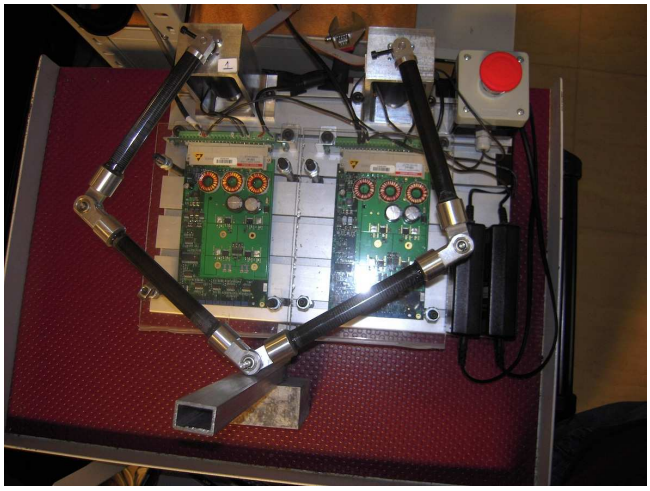

Figure 5.30: Pantograph contact experiment setup

In both artificial and internet delay experiments, it is observed that the slave system tracks the trajectory of the master pantograph successfully with a maximum error of 0.1 *rad* for the 1-DOF manipulators and 2.5 *cm* for the pantographs. It is also shown by the results that the proposed architecture and delay compensation method is robust to the unpredictable delay and low-sampling problems introduced by internet communication. Stable and force reflecting teleoperation is achieved in all experiments.

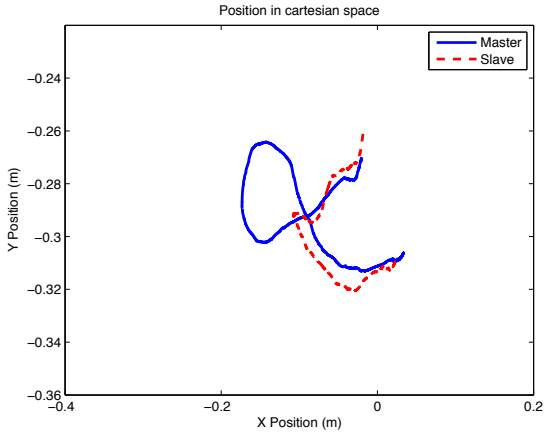

Figure 5.31: Pantograph contact experiment: Point contact

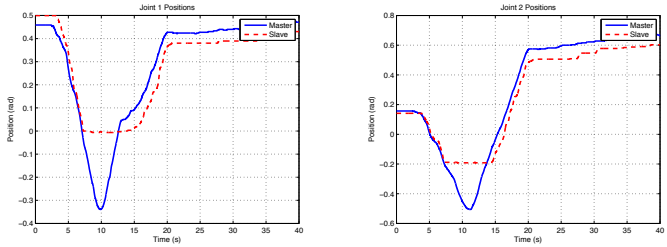

Figure 5.32: Joint positions

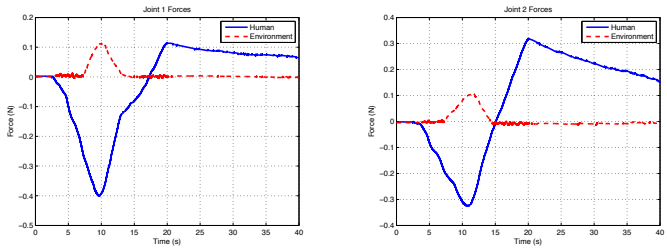

Figure 5.33: External forces on the joints

Chapter VI

6 Conclusion and Future Work

In this thesis, an observer based delay compensation method for linear and nonlinear bilateral teleoperation systems is proposed. The necessity for consideration of nonlinear tele-operators arises from the fact that nonlinear robots are commonly used in many modern tele-robotics applications to handle complex tasks and will be more so in the future. The method involves three observers: Predictor observer, disturbance observer and reaction torque observer. A novel predictor observer (PROB) is developed, its stability is shown by a Lyapunov analysis and it is shown that it estimates the future states of the remote manipulator. These estimations are fed to the controller of the remote manipulator so that the control input can be computed at the local site and sent through the communication channel, separating the approach proposed in this work from the commonly used passivity based techniques in the literature. The proposed method provides a robust control architecture that delivers stable and force reflecting bilateral teleoperation under unpredictable internet delay conditions. The systems are run by acceleration control that consists of a Proportional-Derivative control over the error between master position and estimated position of the slave and a Proportional control over the estimated operator and environment forces. The stability of the control inputs for both the local and remote operators are

shown in a Lyapunov framework.

The performance of the proposed method is verified with simulations and compared to two other techniques in the literature. It is further tested with experiments performed under variable delay generated in the Matlab/Simulink environment and real internet delay by bouncing signals between the Sabancı University campus and Beşiktaş on two different testbeds: linear 1-DOF robot arms and nonlinear 2-DOF pantograph robots. The proposed method performs successfully in both the simulations and experiments, delivering stable and force reflecting teleoperation under delay conditions. Its advantages over the two other methods in stability and force reflection are demonstrated in the simulations. It is shown in the experiments that the proposed method is robust to the sampling rate problems introduced by the internet connection.

The robustness of the proposed method can be further tested with longer delays over greater distances and different manipulators with more degrees of freedom. In future experiments, the exchanged signals can be bounced off a computer in a different country or even continent to analyze the effects on the stability and force reflection of the system. The 2-DOF pantograph robots can be changed with 6-DOF robotic manipulators, also linearized using DOBs, and the effectiveness of the PROB in estimating the states of these manipulators can be investigated. Another direction in this research can be to modify the predictor observer to incorporate a nonlinear model of the remote system. This approach can improve the tracking performance of the remote system since the accuracy of state predictions will not only rely on the effectiveness of the DOBs in linearizing the system. Finally, the symmetric nature of the bilateral system can be changed by employing the

position and force scaling techniques in the literature or developing novel ones. In a realistic bilateral teleoperation system, the need to control a 6-DOF industrial robot arm is a very acceptable condition and relying on an identical manipulator as a master system is both expensive and impractical. Forming a bilateral teleoperation system that consists of a master desktop system such as the PHANTOM Desktop or a simple joystick and a slave 6-DOF manipulator is more feasible but requires position and force scaling methods to compensate for the difference in their sizes and workspaces.

Appendix A

Nonlinear Damping Property

Nonlinear damping property can be described as completing the square operation. The last two terms of Equation (3.24)

$$K_{f_m} r_m e_f - k_{2m} K_{f_m}^2 r_m^2$$

can be simplified to

$$-k_{2m} K_{f_m}^2 (r_m^2 - \frac{1}{k_{2m} K_{f_m}} r_m e_f)$$

and the terms inside the parantheses can be completed to a difference of squares

$$-k_{2m} K_{f_m}^2 [(r_m - \frac{1}{2k_{2m} K_{f_m}} e_f)^2 - \frac{1}{4k_{2m}^2 K_{f_m}^2} e_f^2]$$

then the parantheses can be distributed to yield

$$\frac{1}{4k_{2m}} e_f^2 - \underbrace{k_{2m} K_{f_m}^2 (r_m - \frac{1}{2k_{2m} K_{f_m}} e_f)^2}_{\geq 0}$$

since the last term of the this expression is always greater than or equal to 0, provided that $k_{2m} \geq 0$, the inequality

$$K_{f_m} r_m e_f - k_{2m} K_{f_m}^2 r_m^2 \leq \frac{1}{4k_{2m}} e_f^2$$

can be formed which can be further simplified to

$$K_{f_m} r_m e_f - k_{2m} K_{f_m}^2 r_m^2 \leq \frac{1}{k_{2m}} e_f^2$$

as used in Equation (3.25).

References

[1] T. Sheridan, W. Ferrell , "Remote Manipulative Control with Transmission Delay", IEEE Transactions on Human Factors in Electronics, vol. 4, pp. 25-29, 1963.

[2] W. Ferrell, "Remote Manipulation with Transmission Delay", IEEE Transactions on Human Factors in Electronics", vol. 6, pp. 24-32, 1965.

[3] W. Ferrell, "Delayed Force Feedback", IEEE Transactions on Human Factors in Electronics, pp. 449-455, 1966.

[4] R. Anderson and M. Spong, "Bilateral Control of Teleoperators with Time Delay", IEEE Conference on Decision and Control, pp. 167-173, 1988.

[5] R. Anderson and M. Spong, "Asymptotic Stability for Force Reflecting Teleoperators with Time Delay", IEEE Transactions on Autumation and Control, pp. 1618-1625, 1989.

[6] G. Niemeyer, J. Slotine, "Stable Adaptive Teleoperation", IEEE Journal of Oceanic Engineering, vol. 16, no. 1, pp. 152-162, 1992.

[7] G. Niemeyer, J. Slotine, "Transient Shaping in Force-Reflecting Teleoperation", Internation Conference on Advanced Robotics, vol. 1, pp. 261-266, Pisa, Italy, June 1991.

[8] K. Kosuge, H. Murayama, K. Takeo, "Bilateral Feedback Control of Telemanipulators via Computer Network", IEEE/RSJ International Conference on Intelligent Robots and Systems, vol. 3, pp. 1380-1385, Osaka, Japan, November 1996.

[9] R. Oboe and P. Fiorini, "Internet-Based Telerobotics: Problems and Approaches", International Conference of Advanced robotics, pp. 765-770, Monterey, USA, 1997.

[10] R. Oboe and P. Fiorini, "A Design and Control Environment for Internet-Based Telerobotics", The International Journal of Robotics Research, vol. 17, pp. 433-449, 1998.

[11] G. Niemeyer, J. Slotine, "Towards Force-Reflecting Teleoperation Over the Internet", IEEE International Conference on Robotics and Automation, vol. 3, pp. 1909-1915, Leuven, Belgium, May 1998.

[12] R. Lozano, N. Chopra, M. Spong, "Passivation Of Force Reflecting Bilateral Teleoperators with Time Varying Delay", Mechatronics Forum International Conference, pp. 24-26, Entschede, Netherlands, June 2002.

[13] N. Chopra, M. Spong, S. Hirche, M. Buss, "Bilateral Teleoperation Over the Internet: The Time Varying Delay Problem", American Control Conference, vol. 1, pp. 155-160, Denver, Colorado, June 2003.

[14] N. Chopra, M. Spong, R. Lozano, "Adaptive Coordination Control of Bilateral Teleoperators with Time Delay", IEEE Conference on Decision and Control, pp. 4540-4547, Paradise Island, Bahamas, December 2004.

[15] C. Secchi, S. Stramigioli, C. Fantuzzi, "Dealing with Unreliabilities in Digital Passive Geometric Telemanipulation", IEEE/RSJ International Conference on Intelligent Robots and Systems, vol. 3, pp. 2823-2828, Las Vegas, USA, October 2003.

[16] P. Beretesky, N. Chopra, M. Spong, "Discrete Time Passivity in Bilateral Teleoperation Over the Internet", IEEE International Conference

on Robotics and Automation, vol. 5, pp. 4557-4564, New Orleans, USA, April 2004.

[17] S. Mastellone, D. Lee, M. Spong, "Master-Slave Synchronization with Switching Communication Through Passive Model-Based Control Design", American Control Conference, pp. 3203-3208, Minneapolis, USA, June 2006.

[18] J. Park, H. Cho, "Sliding-Mode Montroller for Bilateral Teleoperation with Varying Time Delay", IEEE/ASME International Conference on Advanced Intelligent Mechatronics, pp.311-316, Atlanta, USA, September 1999.

[19] H. Cho, J. Park, K. Kim, J. Park, "Sliding-Mode-Based Impedance Controller for Bilateral Teleoperation Under Varying Time-Delay", IEEE International Conference on Robotics and Automation, v. 1, pp. 1025-1030, Seoul, Korea, May 2001.

[20] N. Chopra, M. Spong, "Synchronization of Networked Passive Systems with Applications to Bilateral Teleoperation", Society of Instrumentation and Control Engineering of Japan, Okayama, Japan, August 2005.

[21] D. Lee, M. Spong, "Bilateral Teleoperation of Multiple Cooperative Robots Over Delayed Communication Networks: Theory", IEEE International Conference on Robotics and Automation, pp. 360-365, Barcelona, Spain, April 2005.

[22] D. Lee, M. Spong, "Passive Bilateral Teleoperation with Constant Time-Delays", IEEE International Conference on Robotics and Automation, pp. 2902-2907, Orlando, USA, May 2006.

[23] E. Nuno, R. Ortega, N. Barabanov, L. Basanez, "A Globally Stable PD Controller for Bilateral Teleoperators", IEEE Transactions on Robotics, vol. 23, no. 3, pp. 753-758, 2008.

[24] E. Nuno, L. Basanez, R. Ortega, M. Spong , "Position Tracking for Nonlinear Teleoperators with Variable Time Delay", International Journal of Robotics Research, vol. 28, no. 7, pp. 895-910, 2009.

[25] D. Lawrence, "Stability and Transparency in Bilateral Teleoperation", IEEE Transactions on Robotics and Automation, vol. 9, no. 5, pp. 624-637, October 1993.

[26] Y. Yokokohji, T. Yoshikawa, "Bilateral Control of Master Slave Manipulators for Ideal Kinesthetic Coupling Formulation and Experiment", IEEE Transactions on Robotics and Automation, vol. 10, no. 5, pp. 605-620, 1994.

[27] M. Zhu, S. Salcudean, "Achieving Transparency for Teleoperator Systems Under Position and Rate Control", IEEE/RSJ International Conference on Intelligent Robots and Systems, vol. 2, pp. 7-12, Pittsburgh, USA, August 1995.

[28] K. Hashtrudi-Zaad, S. Salcudean, "Adaptive Transparent Impedance Reflecting Teleoperation", IEEE International Conference on Robotics and Automation, pp. 1369-1374, Minneapolis, USA, April 1996.

[29] K. Hashtrudi-Zaad, S. Salcudean, "On the Use of Local Force Feedback for Transparent Teleoperation", IEEE International Conference on Robotics and Automation, pp.1863-1869, Detroit, Michigan, May 1999.

[30] O. Smith, "A Controller to Overcome Dead Time", International Society of Automation Journal, vol. 6, no. 2, pp. 28-33, 1959.

[31] H. Arioui, S. Mammar and T. Hamel, "A Smith Prediction Based Haptic Feedback Controller for Time Delayed Virtual Environments Systems", American Control Conference, pp. 4303-4308, Anchorage, USA, May 2002.

[32] S. Munir, W. Book, "Wave-Based Teleoperation with Prediction", American Control Conference, pp. 4605-461, Arlington, USA, June 2001.

[33] S. Munir and W. Book, "Internet-Based Teleoperation Using Wave Variables with Prediction", IEEE/ASME Transactions on Mechatronics, vol. 7, no. 2, pp. 124-133, 2002.

[34] A. Shahdi, S. Sirouspour, "A Multi-Model Decentralized Controller for Teleoperation with Time Delay", IEEE/RSJ International Conference on Intelligent Robots and Systems, pp. 496-501, San Diego, USA, October 2007.

[35] A. Shahdi, S. Sirouspour, "Improved Transparency in Bilateral Teleoperation with Variable Time Delay", IEEE/RSJ International Conference on Intelligent Robots and Systems, pp. 4616-4621, Saint Louis, USA, October 2009.

[36] A. Shahdi, S. Sirouspour, "An Adaptive Controller for Bilateral Teleoperation Under Time Delay", IEEE EuroHaptics Conference and Symposium on Haptic Interfaces for Virtual Environment and Teleoperator Systems, pp. 308-313, Salt Lake City, USA, March0 2009.

[37] B. Gadamsetty, S. Bogosyan, M. Gökaşan, A. Şabanoviç, "Novel Observers for Compensation of Communication Delay in Bilateral Control Systems", IEEE Conference on Industrial Electronics, pp. 3019-3026, Porto, Portugal, November 2009.

[38] F. Mobasser, K. Hashtrudi-Zaad, "A Model-Independent Force Observer for Teleoperation Systems", IEEE International Conference on Mechatronics and Automation, vol. 2, pp. 964-969, Niagara Falls, Canada, July 2005.

[39] A. Smith, F. Mobasser, K. Hashtrudi-Zaad, "Neural-Network-Based Contact Force Observers for Haptic Applications", IEEE Transactions on Robotics, vol. 22, no. 6, pp. 1163-1175, 2006.

[40] I. Polushin, P. Liu, C. Lung, "Projection-Based Force Reflection Algorithm for Stable Bilateral Teleoperation Over Networks", IEEE/RSJ International Conference on Intelligent Robots and Systems, pp. 2654-2659, San Diego, USA, October 2007.

[41] I. Polushin, P. Liu, C. Lung, "Projection-Based Force Reflection Algorithm for Stable Bilateral Teleoperation Over Networks", IEEE Transactions on Instrumentation and Measurement, vol. 58, no. 9, pp. 1854-1865, 2008.

[42] J. Daly, W. Wang, "Bilateral Teleoperation Using Unknown Input Observers for Force Estimation", American Control Conference, pp. 89-95, Saint Louis, USA, June 2009.

[43] K.Natori, T.Tsuji, K.Ohnishi, A.Hace, K.Jezernik, "Robust Bilateral Control with Internet Communication", IEEE Conference on Industrial Electronics, Busan, Korea, vol. 3, pp.2321-2326, November 2004.

[44] K.Natori, T.Tsuji, K.Ohnishi, "Time Delay Compensation by Communication Disturbance Observer in Bilateral Teleoperation System", IEEE International Workshop on Advanced Motion Control, pp. 218-223, Istanbul, Turkey, March 2006.

[45] K.Natori, R. Oboe, K.Ohnishi, "Analysis and Design of Time Delayed Control Systems with Communication Disturbance Observer", IEEE International Symposium on Industrial Electronics, pp. 3132-3137, Vigo, Spain, June 2007.

[46] N. Iiyama, K.Natori, K.Ohnishi, "Bilateral Teleoperation Under Time-Varying Communication Time Delay Considering Contact with Environment", Electronics and Communications in Japan, vol. 92, no. 7, 2009.

[47] T. Murakami, F. Yu, K. Ohnishi, "Torque Sensorless Control in Multi Degree-of-Freedom Manipulator", IEEE Transactions on Industrial Electronics, vol. 40, no. 2, pp. 259-265, 1993.

[48] K. Natori, T. Tsuji, K. Ohnishi, A. Hace, K. Jezernik, "Time-Delay Compensation by Communication Disturbance Observer for Bilateral Teleoperation Under Time-Varying Delay", IEEE Transactions on Industrial Electronics, vol. 57, no. 3, pp. 1050-1062, 2010.

[49] K. Ohnishi, T. Murakami, "Advanced Motion Control in Robotics", IEEE Conference on Industrial Electronics, vol. 2, pp. 356-359, Philadelphia, USA, November 1989.

[50] K. Eom, I. Suh, W. Chung, S. Oh, "Disturbance Observer Based Force Control of Robot Manipulator without Force Sensor", IEEE International Conference on Robotics and Automation, vol. 4, pp. 1916-1923, Leuven, Belgium, May 1998.

[51] K. Hashtrudi-Zaad, S. Salcudean, "Analysis of Control Architectures for Teleoperation Systems with Impedance/Admittance Master and Slave Manipulators", International Journal of Robotics Research, vol. 20, no. 6, pp. 419-445, 2001.

[52] W. Zhu, S. Salcudean, "Teleoperation with Adaptive Motion/Force Control", IEEE International Conference on Robotics and Automation, pp.231-237, Detroit, MI, May 1999.

[53] V. Utkin, J. Guldner, J. Shi, "Sliding Mode Control in Electromechanical Systems", pp. 33, CRC Press, Boca Raton, 1999.

[54] T. Leblebici, "Delay Compensation in Bilateral Teleoperation Using Predictor Observers", pp. 62-66, Master Thesis, Sabancı University, 2010.